

https://dspace.org/

Comparison of code rate and transmit diversity in MIMO systems

Churms, Duane

2016

http://hdl.handle.net/10539/21155

Churms, Duane (2016) Comparison of code rate and transmit diversity in MIMO systems, University of Witwatersrand, Johannesburg, <http://wiredspace.wits.ac.za/handle/10539/21155>

Downloaded from a DSpace repository. https://dspace.org/

University of the Witwatersrand,
Johannesburg

Masters Thesis

Comparison of Code Rate and Transmit Diversity in MIMO Systems

Author:
Duane Churms

A thesis submitted in fulfilment of the requirements
for the degree of Master of Science

in the

Centre of Excellence in Telecommunications and Software
School of Electrical and Information Engineering

March 2016

The financial assistance of the National Research Foundation (NRF) towards this research is hereby acknowledged. Opinions expressed and conclusions arrived at, are those of the author and are not necessarily to be attributed to the NRF.

Declaration of Authorship

I, Duane Churms, declare that this thesis titled, 'Comparison of Code Rate and Transmit Diversity in MIMO Systems' and the work presented in it are my own. I confirm that:

- This work was done wholly or mainly while in candidature for a research degree at this University.
- Where any part of this thesis has previously been submitted for a degree or any other qualification at this University or any other institution, this has been clearly stated.
- Where I have consulted the published work of others, this is always clearly attributed.
- Where I have quoted from the work of others, the source is always given. With the exception of such quotations, this thesis is entirely my own work.
- I have acknowledged all main sources of help.
- Where the thesis is based on work done by myself jointly with others, I have made clear exactly what was done by others and what I have contributed myself.

Signed: _____

Date: _____

UNIVERSITY OF THE WITWATERSRAND, JOHANNESBURG

Abstract

Engineering and the Built Environment
School of Electrical and Information Engineering

Master of Science

Comparison of Code Rate and Transmit Diversity in MIMO Systems

by Duane Churms

Supervisor: Dr. Jaco Versfeld

In order to compare low rate error correcting codes to MIMO schemes with transmit diversity, two systems with the same throughput are compared. A VBLAST MIMO system with $(15, 5)$ Reed-Solomon coding is compared to an Alamouti MIMO system with $(15, 10)$ Reed-Solomon coding. The latter is found to perform significantly better, indicating that transmit diversity is a more effective technique for minimising errors than reducing the code rate. The Guruswami-Sudan/Koetter-Vardy soft decision decoding algorithm was implemented to allow decoding beyond the conventional error correcting bound of RS codes and VBLAST was adapted to provide reliability information. Analysis is also performed to find the optimal code rate when using various MIMO systems.

Acknowledgements

I would like to thank my fiancée and my parents for their enduring love and support. I would also like to thank my supervisor for the many valuable discussions we had.

Contents

Declaration of Authorship i

Abstract ii

Acknowledgements iii

Contents iv

List of Figures vi

List of Tables vii

Abbreviations viii

Symbols x

1 Introduction 1
- 1.1 Research problem . . . 3
- 1.2 Author's contribution . . . 3

2 Literature Survey 5
- 2.1 MIMO channel . . . 5
  - 2.1.1 Rayleigh fading model . . . 8
  - 2.1.2 Interleaving . . . 10
- 2.2 MIMO transmission schemes . . . 11
  - 2.2.1 VBLAST . . . 12
  - 2.2.2 TBLAST . . . 15
  - 2.2.3 Alamouti STBC . . . 16
- 2.3 Reed-Solomon error correcting codes . . . 20
  - 2.3.1 Introduction . . . 20
    - 2.3.1.1 Algebra background . . . 21
    - 2.3.1.2 Error control coding fundamentals . . . 23
  - 2.3.2 Reed-Solomon encoding . . . 24
  - 2.3.3 Reed-Solomon decoding . . . 25
    - 2.3.3.1 Hard decision . . . 25
    - 2.3.3.2 Soft decision . . . 26
    - 2.3.3.3 Guruswami-Sudan algorithm . . . 26

Interpolation 28
Factorisation 35
2.3.3.4 Koetter-Vardy algorithm 39

3 Research Methodology **42**
3.1 Experimental setup 42
3.2 System description 44
3.2.1 Reed-Solomon 44
3.2.2 MIMO schemes 46
3.2.3 Modulation and channel model 47

4 Results **49**
4.1 Optimal code rates 49
4.2 VBLAST vs TBLAST 54
4.3 Soft decision decoding gain 56
4.4 Transmit diversity vs code rate 59

5 Conclusion **62**
5.1 Optimal code rates 62
5.2 VBLAST vs TBLAST 63
5.3 Soft decision decoding gain 64
5.4 Code rate vs transmit diversity 64
5.5 Recommendations for future work 65

Bibliography **67**

List of Figures

2.1 Simplified block diagram of simulated system 5
2.2 Simplified signal paths for a 2×2 MIMO system 7
2.3 Interleaver structure showing ordering of transmitted symbols 11
2.4 16-QAM constellation with one reliable and one unreliable symbol 27
2.5 Flow diagram from demodulator output to final output message 28
2.6 Comparison of the error correcting bounds for the Guruswami-Sudan and Berlekamp-Massey algorithms. Codeword length $n = 15$. 29
2.7 Relationship between root multiplicities and derivatives 31
2.8 Tree representation of Roth-Ruckenstein output 38

3.1 System Overview 44

4.1 Comparison of code rates in an AWGN environment 51
4.2 Comparison of code rates in a SISO Rayleigh environment 51
4.3 Comparison of code rates in an Alamouti MIMO environment 52
4.4 Comparison of code rates in a VBLAST MIMO environment 53
4.5 Comparison of code rates in a TBLAST MIMO environment 54
4.6 Comparison of VBLAST and TBLAST using the Berlekamp-Massey decoding algorithm 55
4.7 Comparison of VBLAST and TBLAST using a 2×2 MIMO system and the Koetter-Vardy decoding algorithm 56
4.8 Comparison of soft and hard decision RS decoding with the Alamouti scheme 57
4.9 Comparison of soft and hard decision RS decoding with the VBLAST scheme 58
4.10 Comparison of soft and hard decision RS decoding with the TBLAST scheme 59
4.11 Comparison of MIMO systems with equal overall rate 60

List of Tables

2.1 VBLAST transmission over two antennas 13
2.2 Alamouti encoding scheme 19
2.3 Received symbol notation 19
2.4 Data generated at each recursion step 38

3.1 Alamouti STBC structure 47

4.1 Summary of soft decision gains at SER = 10^{-4} 58

Abbreviations

AWGN	Additive White Gaussian Noise
CAI	Co-Antenna Interference
CSI	Channel State Information
dB	Decibel
DBLAST	Diagonal Bell Labs Layered Space-Time Architecture
FEC	Forward Error Correction
FT	Feng-Tzeng
GF	Galois Field
GS	Guruswami-Sudan
HD	Hard Decision
Hz	Hertz
ISI	Inter Symbol Interference
KV	Koetter-Vardy
LOS	Line of Sight
LTE	Long Term Evolution
MDS	Maximum Distance Separable
MIMO	Multiple Input Multiple Output
MRC	Maximal Ratio Combining
QAM	Quadrature Amplitude Modulation
RR	Roth-Ruckenstein
RS	Reed-Solomon
RX	Receive
SD	Soft Decision
SER	Symbol Error Rate
SISO	Single Input Single Output

SNR	Signal to Noise Ratio
STBC	Space Time Block Code
TBLAST	Turbo Bell Labs Layered Space-Time Architecture
TX	Transmit
VBLAST	Vertical Bell Labs Layered Space-Time Architecture

Symbols

E_s	Energy per symbol
f_d	Doppler spread
h_{ij}	Channel path from TX antenna j to RX antenna i
n_T	Number of transmitting antennas
n_R	Number of receiving antennas
N_0	Noise spectral density
$\mathbf{H}$	Channel transfer matrix
k	Number of message symbols per codeword
n	Number of symbols per codeword
$\mathbf{n}$	Noise vector
$\mathbf{r}$	Received vector
R_M	Rate of MIMO scheme
R_E	Rate of FEC code
T_0	Channel coherence time
T_{fade}	Block fading period
T_s	Symbol period
V	Velocity
W	Bandwidth
$\mathbf{x}$	Transmitted vector
λ	Wavelength

Chapter 1

Introduction

In conventional wireless communication, a single transmitting antenna sends information to a single receiving antenna. While this is effective when a line of sight (LOS) path is present, obstructions between the transmitter and receiver can severely hamper the performance of the system. The primary effect of obstructions in the LOS path is that the signal travelling along the LOS path is attenuated. As a result, the majority of the total signal power at the receiver is courtesy of the signal travelling along paths that involve at least one reflection [1].

Since the reflected paths may have a different number of reflecting surfaces and different path lengths, the phase at which each path's signal arrives is different. In the ideal scenario, the phases are all identical, creating constructive interference. This maximises the signal to noise ratio at the receiver. In the worst case, however, the signals interfere destructively at the receiving antenna, resulting in a very poor SNR. This phenomenon is known as multipath fading.

A technique to combat multipath fading is receive diversity, where multiple antennas are employed at the receiver. The antennas are spaced a minimum of half a wavelength apart to ensure that the paths are sufficiently uncorrelated [2]. While one receiving antenna may be experiencing destructive interference, the rest should experience more favourable conditions. The signals from the antennas can then be combined to recover the transmitted signal with greater confidence.

The natural extension to receive diversity is transmit diversity. Since additional paths can be created by adding antennas at the receiver, a similar effect can be achieved by

adding transmitting antennas. If the same symbol is transmitted over different antennas in different time slots, it is more likely to be transmitted over a good channel path.

When multiple antennas are employed at both the transmitter and the receiver, it is called a Multiple Input Multiple Output (MIMO) system. The additional transmit antennas do not have to be used for diversity, though. Some MIMO schemes utilise the additional paths to transmit multiple symbols per time slot, increasing the rate and spectral efficiency of the system [3].

Another technique for error prevention that has been widely used in Single Input Single Output (SISO) systems is channel coding, more specifically error correction coding. Error correcting codes transmit parity symbols in addition to the information symbols to form codewords. When errors occur in either the information or the parity symbols, the code attempts to recover the transmitted codeword. Additional parity symbols allow more errors to be corrected per codeword, but this also lowers the rate of the code. A smaller fraction of the total energy required to transmit the codeword is thus allocated to transmitting the information symbols.

Not all error correcting codes offer the same error correcting capability, though. The upper bound for error correcting capability using conventional decoding is half the number of parity symbols [4]. Most error correcting codes, however, do not achieve this bound. One family of codes to achieve this bound is Reed-Solomon codes [5].

In order to correct errors beyond this bound, soft decision (SD) decoding must be used [6]. In hard decision (HD) decoding, the demodulator only passes the most likely symbol to the decoder. For SD decoding, however, the demodulator passes reliability information to the decoder as well. The SD decoder can then place more emphasis on the most reliable symbols while minimising the effect of the unreliable symbols. Consider a grossly oversimplified example where the errors in a received codeword all have low reliability, while the correct symbols have high reliability. A soft decision decoder could theoretically correct one error for every parity symbol by ignoring all the low reliability symbols. This special case is analogous to erasure decoding, but a true SD decoder handles a wide range of reliabilities.

1.1 Research problem

Transmit diversity and error correction codes typically reduce the number of errors by lowering the rate at which information symbols are transmitted. Transmit diversity is achieved by retransmitting symbols or permutations of symbols, which reduces the overall rate of the system. Higher transmit diversity results in lower error rates at the demodulator output, since there are independent samples from which to generate the decision statistics. Error correcting codes essentially spread the information from k information symbols over n information symbols. Low rate codes are capable of correcting more errors than high rate codes of the same type, resulting in fewer errors at the decoder output. Transmit diversity is inversely related to the overall rate of the system, while code rate is directly proportional to the overall rate.

The research problem is stated as follows:

> Investigate the feasibility of using low rate channel codes as an alternative to transmit diversity in MIMO systems.

The proposed research is to compare two types of MIMO systems with the same overall rate. The one type of system will use a high rate channel code in conjunction with a low rate (i.e. high diversity) MIMO scheme, while the other type will use a low rate channel code with a high rate (low diversity) MIMO scheme. The feasibility of the schemes will be based on the $\frac{E_s}{N_0}$ required to achieve a symbol error rate of 10^{-4}.

1.2 Author's contribution

The author's contribution can be divided into programming and analysis. Programming was performed in MATLAB [7]. The following components were used directly from the Statistics and Communications toolboxes:

1. Additive white Gaussian noise (AWGN),
2. Systematic Reed-Solomon encoding, and
3. Berlekamp-Massey hard decision Reed-Solomon decoding.

The remainder of the components were implemented by the author:

1. Guruswami-Sudan list decoding algorithm,
2. Koetter-Vardy multiplicity selection algorithm,
3. VBLAST MIMO encoding and decoding,
4. TBLAST MIMO encoding and decoding,
5. Alamouti STBC encoding and decoding, and
6. Block fading Rayleigh channel.

The author designed the experiments to answer the research problem and generate the three additional sets of results. All analysis of the results that were generated was also performed by the author.

This document is structured as follows: Chapter 2 contains the literature survey, including discussions on the MIMO channel, MIMO transmission schemes and Reed-Solomon coding. Chapter 3 outlines the research methodology used to address the research problem and describes the experimental setup. The results generated in this research are presented and analysed in Chapter 4. Final conclusions are drawn in Chapter 5.

Chapter 2

Literature Survey

The system can be broadly divided into three areas: the MIMO channel, the MIMO transmission scheme and the error correcting channel code, as shown in figure 2.1. The literature survey is correspondingly divided into three sections – the MIMO channel is discussed in section 2.1. Various techniques of transmitting information over a MIMO channel are then investigated in section 2.2. Finally, error correction coding is discussed in section 2.3, including advanced decoding techniques.

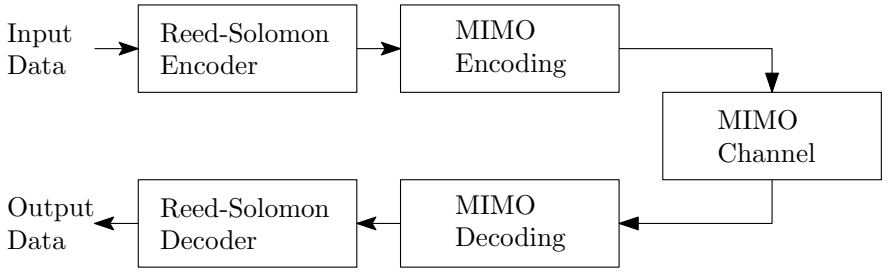


FIGURE 2.1: Simplified block diagram of simulated system

2.1 MIMO channel

When a signal propagates from a transmitter to a receiver, the ideal scenario is when line of sight is available. The signal remains relatively undistorted and minimally attenuated due to travelling along a direct path. When there is no line of sight path, the signal is reflected, refracted and attenuated by various objects.

Under these conditions the signal can arrive at the receiver via several different paths. These paths can have different attenuations and phase shifts dependent on the objects encountered and the total path length. The different phase shifts can cause the paths to interfere with each other either constructively or destructively. When the signals interfere destructively, the received signal to noise ratio drops significantly. This phenomenon is known as multipath fading [8].

Multipath fading is not to be confused with shadowing, which can also cause very low SNRs. Shadowing is due to a large obstruction such as a mountain attenuating the signal. There are no reflected signal paths by which sufficient energy from the transmitter can reach the receiver. In order to overcome shadowing, either the transmitter or the receiver must move so that the obstruction no longer blocks the signal. For multipath fading the transmitter or receiver may only need to move on the order of a single wavelength in order to eliminate the destructive interference.

Receive diversity is one option for dealing with multipath fading. Multiple antennas are placed at the receiver, spaced at least half a wavelength apart [2, 9]. Due to the signal paths having differing angles of arrival, some of the antennas will experience destructive interference while other antennas will experience constructive interference. The transmitted symbol can then be recovered from the multiple samples at the receive antennas using techniques such as maximal ratio combining (MRC) [10].

Multiple antennas can also be employed at the transmitter – this actually exploits the multipath property of the channel to achieve greater capacity. Provided that the system is in a rich scattering environment and that the antennas are spaced sufficiently, the channel path between each pair of antennas is uncorrelated enough to allow an independent data stream to be transmitted from each antenna [11]. The additional data streams can alternatively be used to transmit redundant data streams, thus increasing transmitter diversity.

Wolniansky and Foschini demonstrated that systems with a very large number of antennas can offer extraordinary capacity [11]. At an average SNR of 21 dB, a single antenna at the transmitter and receiver offers 1.2 bits/cycle. Using two, four or sixteen antennas at each end allows capacities up to 7, 19 and 88 bits/cycle. It would thus be ideal to fit as many antennas into a system as possible.

Selecting the number of antennas to use for a system is largely limited by the physical space available in the device. Antennas should be spaced by at least half a wavelength. If they are closer together, the channel paths become highly correlated and the system can no longer exploit the multipath properties [11]. At a frequency of 2 GHz, half a wavelength corresponds to approximately 7 cm. Due to space limitations in user equipment such as cellphones, two antennas are most common. That said, the WiFi specification allows for up to four antennas [12, 13], while LTE allows for up to an 8×8 configuration for download links [14]. In this case cross-polarised antennas are used to keep channel paths uncorrelated without requiring excessive space [15]. The system simulated for this research consists of two transmitting and two receiving antennas, as shown in figure 2.2. The 2×1 received vector $\mathbf{r}$ is given by

$$\mathbf{r} = \mathbf{H}\mathbf{x} + \mathbf{n} \,, \tag{2.1}$$

where $\mathbf{H}$ is the 2×2 channel matrix, $\mathbf{x}$ is the 2×1 transmitted vector and $\mathbf{n}$ is the 2×1 noise vector. The channel matrix $\mathbf{H}$ represents the individual paths between antenna pairs such that

$$\mathbf{H} = \begin{bmatrix} h_{11} & h_{12} \\ h_{21} & h_{22} \end{bmatrix} ,$$

where h_{ij} is a complex value representing the magnitude and phase shift of the path from transmitting antenna j to receiving antenna i.

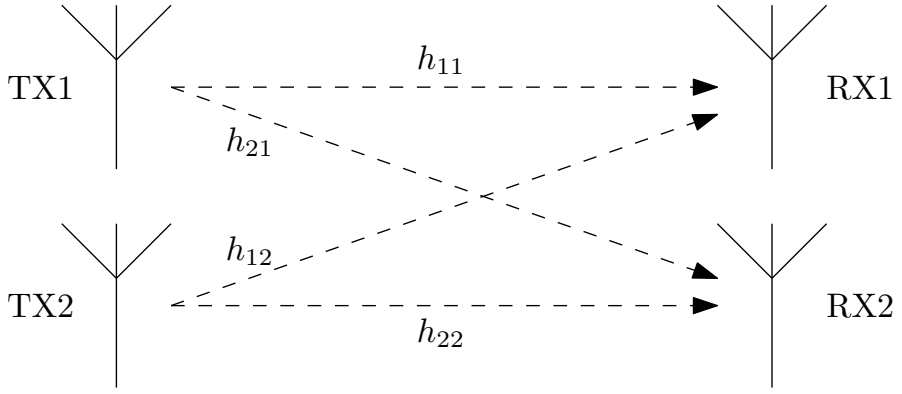


FIGURE 2.2: Simplified signal paths for a 2×2 MIMO system

Objects such as walls reflect the radio waves travelling from the transmitter to the receiver, causing changes in phase and angle of arrival of the waves. The signal propagates along a slightly different path for each antenna pair. Channel paths are thus of different lengths and experience different levels of attenuation. The channel entries h_{ij}

are complex numbers indicating the phase and magnitude change introduced by each of the channel paths. The exact values of the channel entries used in simulations are determined by the channel model used.

2.1.1 Rayleigh fading model

The Rayleigh fading model [16] was initially developed to model over-the-horizon communications, where scattering is due to the ionosphere and troposphere [8]. In built up areas, mobile digital communications systems experience large amounts of scattering due to radio waves reflecting off of buildings. Buildings also often obstruct the line of sight, resulting in the majority of the received signal power being from reflected waves. Although the Rayleigh fading model was not explicitly designed for such an environment, it provides a good approximation of the fading effects [2]. This was verified by Chizhik et al. [17] by means of measurements taken in Manhattan. The Rayleigh fading model is also a good approximation of fading in indoor environments, as demonstrated by Nishimoto [18].

The fundamental property of the Rayleigh fading model is that each channel path is a Rayleigh distributed random variable. The real and imaginary components of a Rayleigh random variable are Gaussian distributed with zero mean. Using the rate at which these random variables change, Rayleigh channels can be classified into one of three categories: slow fading, fast fading and block fading.

A slow fading channel is characterised by

$$T_0 > T_s \text{ [8]}, \tag{2.2}$$

where T_s is the time taken to transmit one symbol and T_0 is the coherence time of the channel, or the time during which the channel remains reasonably constant. This condition can alternatively be stated as

$$W > f_d \text{ [8]}, \tag{2.3}$$

where W is the bandwidth of the system and f_d is the Doppler spread.

The relationship between the coherence time and the Doppler spread is given by

$$T_0 \simeq \frac{\lambda/2}{V} = \frac{0.5}{f_d} \text{ [8]}, \tag{2.4}$$

where V is the relative velocity of the endpoints (or scattering objects) in the direction that the signal is travelling. Considering a system with a 2 GHz carrier frequency and endpoints moving at 120 km/h, the coherence time would thus be 2.25 ms. Unless the transmission rate is slower than about 440 symbols per second, the system will experience slow fading.

Fast fading occurs when the inequalities in equations 2.2 and 2.3 are reversed. The channel is not coherent over even a single symbol period, resulting in the baseband pulse being distorted. This in turn causes synchronisation problems and leads to very high error rates [8]. Fortunately, as seen in the example above, the end points must move very fast or the transmission rate must be very slow to cause a channel to be characterised as fast fading.

Block fading is a simplifying assumption that is often used in research [19, 20]. Instead of the channel varying continuously based on the Doppler frequency, the channel is assumed constant within a fixed time period T_{fade}, which is much longer than T_s. After every T_{fade}, a new channel matrix $\mathbf{H}$ is generated which is independent of all previous channels. The entries h_{ij} of the 2×2 channel transfer matrix $\mathbf{H}$ are independent and identically distributed Rayleigh random variables. These entries have normally distributed real and imaginary components that have zero mean and $\frac{1}{\sqrt{2}}$ variance [11]. The channel matrix is also normalised so that $\mathrm{E}\left[|h_{ij}|^2\right] = 1$ [11]. For the purposes of this research, the channel is modeled as a block fading Raleigh channel.

The $\mathbf{H}$ matrix in a real system would be estimated at the receiver by means of a training sequence or some other channel estimation method [21–24]. This research does not focus on channel estimation or errors in channel estimation. It is thus assumed that the receiver has perfect channel state information (CSI), i.e. the receiver has knowledge of the exact values of all the entries in $\mathbf{H}$.

If some feedback system were employed to allow the transmitter to have CSI, the transmitting power at each antenna could be adjusted to compensate for certain paths having low gain. In this research it it is assumed that no feedback is available, and hence the

transmitter has no CSI. This means that all transmitting antennas operate at the same power level.

2.1.2 Interleaving

When the channel paths are highly correlated the system becomes underdetermined. For example, consider the case where

$$\mathbf{H} = \begin{bmatrix} 1 & 1 \\ 1 & 1 \end{bmatrix} .$$

The set of equations defining the received vector will then be

$$r_1 = x_1 + x_2 + n_1 \text{ , and} \tag{2.5}$$

$$r_2 = x_1 + x_2 + n_2 \text{ .} \tag{2.6}$$

Two noisy copies of the same linear combination of the two transmitted symbols are received. Due to the underdetermined nature of this system, it becomes highly likely that the demodulator will output errors.

When using block fading, a correlated channel matrix causes many errors to occur – an entire fading block could consist solely of errors. This burst of errors would be concentrated within a few error correcting codewords if no interleaver is used. This would result in these codewords containing more errors than the error correction code can correct, resulting in decoding failures.

In order to avoid having large bursts of errors within a single codeword, a block interleaver is used to spread the codewords across multiple fading blocks. The interleaver is designed such that no fading block contributes more than one symbol to any given codeword. This is analogous to a very large interleaver being used in slow fading Rayleigh channels [25]. A diagram of the interleaver is shown in figure 2.3.

The properties of a MIMO channel experiencing multipath fading were discussed in this section. In the next section we introduce various approaches to transmitting information across such a channel.

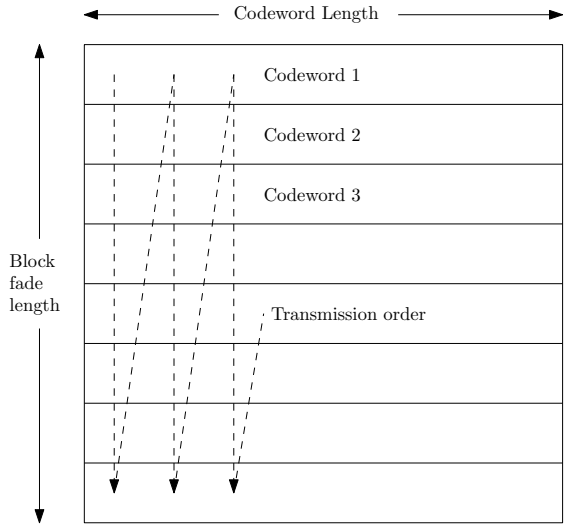


FIGURE 2.3: Interleaver structure showing ordering of transmitted symbols

2.2 MIMO transmission schemes

MIMO systems generally offer benefits in three categories: diversity, spectral efficiency and beamforming [26]. Increased diversity improves the robustness of the system by transmitting each symbol over more than one antenna in separate time slots, mitigating the effect of multipath fading and noise. Higher spectral efficiency, on the other hand, improves overall throughput of the system without increasing the required bandwidth. This is done by transmitting unique symbols over each antenna in all time slots. A third technique, beamforming [27], differs from the previous two categories in that the same symbol is transmitted over multiple antennas in a single time slot. The phases at each antenna are adjusted so that the signals interfere constructively in the intended direction of transmission. This increases the received SNR without increasing the overall transmitted power, and may be used when signal strength is low due to the transmitter and receiver being far apart.

In MIMO schemes that offer diversity or increased spectral efficiency, symbols are transmitted coherently, while in beamforming systems a phase shift is introduced. Beamforming systems will not be considered in this research. Unfortunately it is not possible to maximise both diversity and spectral efficiency within a single MIMO scheme. A high rate scheme, which transmits many symbols per time slot, would provide very good spectral efficiency at the cost of diversity. A low rate scheme on the other hand would require more time slots to transmit the same amount of data, lowering its spectral efficiency but providing very good diversity. Many different MIMO schemes exist which are

designed to achieve one of three things: maximum diversity, maximum spectral efficiency or a trade-off between the two [3, 28–30].

The primary purpose of this research is to investigate the impact of changing the MIMO scheme rate R_M and error correcting code rate R_E while keeping the overall system rate $R = R_M R_E$ constant. The two extremes in terms of MIMO scheme rate are thus investigated, i.e. maximum rate and maximum diversity schemes. Hybrid schemes which attempt to balance these two parameters were not investigated.

VBLAST and TBLAST are examples of maximum rate MIMO schemes – they are discussed in sections 2.2.1 and 2.2.2. The Alamouti STBC is an orthogonal space-time block code which offers maximum diversity. It is described in section 2.2.3.

2.2.1 VBLAST

One of the earliest MIMO schemes was the Diagonal Bell Laboratories Layered Space-Time architecture (DBLAST), developed by Foschini [9]. It consists of a structure where symbol transmission slots are diagonally layered so that each successive symbol is transmitted on a different antenna. Decoding is also performed on one diagonal layer at a time, which means that the contribution from already decoded layers can be cancelled. Although it offers some diversity, $\frac{n_T(n_T-1)}{2}$ symbol slots are unusable at both the start and the end of a transmission block.

Wolniansky, Foschini et al. proposed an alternative MIMO scheme termed Vertical Bell Laboratories Layered Space-Time architecture (VBLAST) [3]. Instead of performing decoding in diagonal layers, decoding is performed on vertical layers. This eliminates the unusable triangle of transmission slots at the start and end of blocks. This structure offers no diversity, and hence does not allow for cancelling of already decoded layers.

VBLAST can be applied to any number of transmitting antennas, n_T. Transmission involves demultiplexing the input stream into n_T independent substreams. Symbols from each substream are then transmitted coherently by the n_T antennas. The scheme does not require inter-substream coding, although conventional error control coding may be applied to the input stream. Table 2.1 shows an example of the VBLAST scheme for two transmitting antennas.

TABLE 2.1: VBLAST transmission over two antennas

	t_1	t_2	t_3	$\cdots$
TX_1	x_0	x_2	x_4	$\cdots$
TX_2	x_1	x_3	x_5	$\cdots$

The n_R receiving antennas operate in a co-channel fashion, receiving the superimposed signals from all n_T transmitting antennas. The received vector $\mathbf{r}$ of length n_R is thus

$$\mathbf{r} = \mathbf{H}\mathbf{x} + \mathbf{n} \ , \tag{2.7}$$

where $\mathbf{H}$ is the $n_R \times n_T$ channel transfer matrix, $\mathbf{x}$ is the $n_T \times 1$ transmitted vector and $\mathbf{n}$ is the $n_R \times 1$ AWGN noise vector.

VBLAST decoding involves decoding a single symbol at a time. Symbols that have not yet been decoded are treated as if they are zero – this is known as zero forcing (ZF) nulling [3]. Zero forcing is done by choosing a weight vector of length n_R notated $\mathbf{w}_i$, where $1 < i < n_T$, such that

$$\mathbf{w}_i(\mathbf{H})_j = \delta_{ij} \ , \tag{2.8}$$

where $(\mathbf{H})j$ is the jth column of $\mathbf{H}$ and δ_{ij} is the Kronecker delta. The product of the two vectors should thus be equal to 1 only when $i = j$, and zero otherwise. The weight vector $\mathbf{w}_i$ is thus the ith row of $\mathbf{G}$, the Moore-Penrose pseudo-inverse [31] of $\mathbf{H}$.

Multiplying the received vector $\mathbf{r}$ by the weight vector $\mathbf{w_i}$ gives the decision statistic y_i:

$$\mathbf{w}_i\mathbf{r} = \mathbf{w}_i\mathbf{H}\mathbf{x} + \mathbf{w}_i\mathbf{n} \tag{2.9}$$

$$\therefore \quad y_i = x_i + \mathbf{w}_i\mathbf{n} \ . \tag{2.10}$$

This approach is known as zero forcing, since each symbol is decoded using the assumption that no other symbol contributes to the received vector. While zero forcing is effective for handling the contribution of undecoded symbols, it is a suboptimal approach when some symbols are already known. In this case, a technique called decision feedback is applied. Once a symbol has been decoded, its contribution to the received vector is cancelled instead of nulled. This is performed by quantising the symbol to the nearest constellation point and then subtracting the expected contribution of that symbol from the received vector.

If this symbol was incorrectly decoded, i.e. quantised to the incorrect constellation point, the error is likely to propagate to the subsequent symbols as well. It is thus important to order the decoding such that the symbols with the largest contribution to the received vector are decoded first. From equation 2.7 it is intuitive that the column of $\mathbf{H}$ with the largest norm will correspond to the symbol with the largest contribution to the received vector. The formal criteria for selecting the decoding order is to decode the symbol with the highest post-detection SNR first [3].

The post-detection SNR (ρ) of the ith symbol is

$$\rho_i = \frac{\mathrm{E}\left[|x_i|^2\right]}{\sigma^2 ||\mathbf{w}_i||^2} \quad [3]. \tag{2.11}$$

Since $\mathbf{w}_i$ is the ith row of $\mathbf{G}$ and the symbols x_i are equiprobable, the symbol order is determined by selecting the row of $\mathbf{G}$ with the smallest norm.

Cancelling is performed in three steps: quantising the decoded symbol, removing its contribution from the received vector and updating the $\mathbf{H}$ matrix. Quantising is simply mapping the decoded point y_{k_i} to the nearest valid point from the QAM constellation of interest, $\hat{x}_{k_i}$. The received vector is adjusted, assuming that the decoded symbol passed through a noiseless channel:

$$\mathbf{r} = \mathbf{r} - \hat{x}_{k_i}(\mathbf{H})_{k_i} \ , \tag{2.12}$$

where $(\mathbf{H})_{k_i}$ is the k_ith column of $\mathbf{H}$. To reflect the fact that the received vector no longer includes the contribution of the k_ith symbol, $\mathbf{H}_{k_i}$ is then set to zero. Since $\mathbf{H}$ changes, $\mathbf{G}_{i+1}$ is also updated by taking the pseudo-inverse of the new $\mathbf{H}$. This process is repeated until all of the symbols have been decoded.

Algorithm 1 provides a summary of the steps involved in VBLAST decoding. Each step is explained below.

1. i is a loop variable which limits the number of iterations to the number of symbols, which is also the number of transmitting antennas.
2. The first version of the received vector is the actual received vector.
3. The first version of $\mathbf{G}$ is initialised to the Moore-Penrose pseudo-inverse of $\mathbf{H}$.
4. The first symbol to be decoded k_1 is chosen based on the row of $\mathbf{G_1}$ with the smallest norm.

Algorithm 1: VBLAST decoding algorithm (from [3])

Data: Channel matrix $\mathbf{H}$ and received vector $\mathbf{r}$
Result: Decoded QAM symbols $\hat{\mathbf{x}}$

$i = 1$
$\mathbf{r_1} = \mathbf{r}$
$\mathbf{G_1} = \mathbf{H}^+$
$k_1 = \underset{j}{\operatorname{argmin}} \, ||(\mathbf{G_1})j||^2$
while $i \leq M$ **do**
  $\mathbf{w_{k_i}} = (\mathbf{G_i})_{k_i}$
  $y_{k_i} = \mathbf{w_{k_i}} \mathbf{r_i}$
  $\hat{x}_{k_i} = Q(y_{k_i})$
  $\mathbf{r_{i+1}} = \mathbf{r_i} - \hat{x}_{k_i}(\mathbf{H})_{k_i}$
  $\mathbf{G_{i+1}} = \mathbf{H}^+_{\mathbf{k_i}}$
  $k_{i+1} = \underset{j \notin \{k_1 \cdots k_i\}}{\operatorname{argmin}} \, ||(\mathbf{G_{i+1}})_j||^2$
  $i = i + 1$
end

5. The loop exits once all symbols have been decoded.

6. The k_ith weight vector for zero forcing nulling is set equal to the row of $\mathbf{G_i}$ corresponding to the symbol to be decoded.

7. The k_ith decision statistic is set equal to the product of the k_ith weight vector and the current received vector.

8. The decision statistic is quantised to the QAM constellation to give the decoded symbol $\hat{x}$.

9. The new version of the received vector is generated by subtracting the contribution of the decoded symbol.

10. The new version of $\mathbf{G}$ is generated by taking the inverse of $\mathbf{H}$ where columns k_1 to k_i have been set to zero.

2.2.2 TBLAST

Turbo-BLAST, or TBLAST, was developed in 2000 by Sellathurai and Haykin [32]. The design objective of TBLAST was to offer improved handling of co-antenna interference (CAI) compared to VBLAST. Even when determining the order of decoded symbols using the post-detection SNR, the likelihood of VBLAST correctly detecting the first symbol is compromised by the interference from symbols which are yet to be decoded.

From a transmission perspective, TBLAST and VBLAST operate identically. Independent symbols are transmitted simultaneously over all n_T antennas. The primary difference between TBLAST and VBLAST is in the way that symbols are recovered. VBLAST operates on a single symbol at a time, multiplying the received vector by the inverse of the channel matrix and then cancelling decoded symbols. TBLAST, on the other hand, makes use of maximal ratio combining (MRC) and iteratively cancels the co-antenna interference.

The decision statistic for the ith symbol contains contributions from three different sources: the desired signal, the contribution from simultaneously transmitted unwanted symbols (CAI) and noise, as shown below.

$$\hat{y}_i = \overbrace{\mathbf{H}_i^H \mathbf{H}_i x_i}^{\text{desired}} + \overbrace{\sum_{j \neq i} \mathbf{H}_i^H \mathbf{H}_j x_j}^{\text{CAI}} + \overbrace{\mathbf{H}_i^H \mathbf{n}}^{\text{noise}} \; . \tag{2.13}$$

If the interfering symbols are known, however, the CAI term of equation 2.13 can be cancelled out completely. Since the actual symbols transmitted cannot be known with complete certainty, the expectation of the symbol $\mathrm{E}[x_i]$ is used. The expectation is calculated using

$$\mathrm{E}[x_i] = \sum_{x_i \in \mathcal{Q}} x_i P(x_i) \; , \tag{2.14}$$

where $\mathcal{Q}$ is the set of constellation points of the modulation scheme.

Equation 2.13 can then be rewritten as

$$\hat{y}_i = \mathbf{H}_i^H \mathbf{H}_i x_i + \sum_{j \neq i} \mathbf{H}_i^H \mathbf{H}_j \left(x_j - \mathrm{E}[x_j] \right) + \mathbf{H}_i^H \mathbf{n} \; . \tag{2.15}$$

The decision statistics and the expectations are iteratively calculated. Once the number of iterations becomes large, $\mathrm{E}[x_j]$ approaches x_j, therefore $(x_j - \mathrm{E}[x_j]) \to 0$. The CAI term from equation 2.13 thus becomes zero, effectively cancelling the co-antenna interference.

2.2.3 Alamouti STBC

Space-time block codes, or STBCs, provide transmit diversity by transmitting different symbols on each antenna, but then transmitting a permutation of those symbols in

subsequent time slots. Symbols and their permutations are typically not transmitted over the same antennas, thus spreading symbols across multiple signal paths. For a given symbol x, the typical permutations that can be transmitted are x, $-x$, x^*, $-x^*$ and scalar multiples of these permutations, where x^* denotes the complex conjugate of x.

One of the advantages of STBCs is that they result in additional equations from which to generate the decision statistics. For example, if the channel is highly correlated as discussed in section 2.1.2, other schemes may only effectively have one equation from which to recover two unknowns. The transmit diversity provided by an STBC will, on the other hand, produce additional equations to resolve the unknowns. These additional equations constitute the transmit diversity.

The main properties of STBCs are diversity, orthogonality and rate. High rate codes typically have low diversity and are unlikely to be orthogonal. Orthogonal codes are desirable because they offer full diversity and allow low complexity decoding [33]. A trade-off therefore has to be made when designing STBCs to achieve a balance between these properties.

The diversity is an indication of the number of unique samples available to the receiver regarding a specific symbol. Each receiving antenna contributes one unique sample irrespective of the MIMO scheme used. The transmitting antennas contribute at most one unique sample per antenna. Full diversity is thus equal to $n_T n_R$.

In order to formally define the diversity of an STBC, it is necessary to first introduce some notation. The symbol transmitted from antenna i at time slot t is given as x_t^i, $i = 1, 2, \cdots, n_t$. Considering an STBC which occupies l time slots, the transmitted codeword can be represented as

$$\mathbf{x} = \begin{bmatrix} x_1^1 & x_1^2 & \cdots & x_1^n \\ x_2^1 & x_2^2 & \cdots & x_2^n \\ \vdots & \vdots & \ddots & \vdots \\ x_l^1 & x_l^2 & \cdots & x_l^n \end{bmatrix}. \tag{2.16}$$

The receiver attempts to decode the received symbols to produce the expected transmitted codeword

$$\hat{\mathbf{x}} = \begin{bmatrix} \hat{x}_1^1 & \hat{x}_1^2 & \cdots & \hat{x}_1^n \\ \hat{x}_2^1 & \hat{x}_2^2 & \cdots & \hat{x}_2^n \\ \vdots & \vdots & \ddots & \vdots \\ \hat{x}_l^1 & \hat{x}_l^2 & \cdots & \hat{x}_l^n \end{bmatrix} . \tag{2.17}$$

It was shown in [33] that the diversity achieved by an STBC is

$$\min_{\mathbf{x},\hat{\mathbf{x}}\in\mathcal{C},\, \mathbf{x}\neq\hat{\mathbf{x}}} \left(\text{rank}\left(\mathbf{B}\left(\mathbf{x},\hat{\mathbf{x}}\right)\right)\right) \times n_R \, , \tag{2.18}$$

where $\mathbf{B}(\mathbf{x},\hat{\mathbf{x}})$ is

$$\mathbf{B}(\mathbf{x},\hat{\mathbf{x}}) = \begin{bmatrix} \hat{x}_1^1 - x_1^1 & \hat{x}_2^1 - x_2^1 & \cdots & \hat{x}_l^1 - x_l^1 \\ \hat{x}_1^2 - x_1^2 & \hat{x}_2^2 - x_2^2 & \cdots & \hat{x}_l^2 - x_l^2 \\ \vdots & \vdots & \ddots & \vdots \\ \hat{x}_1^{n_T} - x_1^{n_T} & \hat{x}_2^{n_T} - x_2^{n_T} & \cdots & \hat{x}_l^{n_T} - x_l^{n_T} \end{bmatrix} . \tag{2.19}$$

The maximum rank of $\mathbf{B}$ that the STBC can achieve across all codeword combinations is naturally $\min(n_T, l)$. This confirms that the maximum diversity that an STBC can achieve is $n_T n_R$.

Orthogonality is a desirable feature in STBC construction, as it ensures that the $\mathbf{B}$ matrix has full rank and is easy to decode [33]. The STBC will thus have full diversity and will eliminate inter symbol interference (ISI). An STBC is orthogonal if the dot product of all pairs of columns is equal to zero.

The rate of an STBC is the number of information symbols that it transmits per time slot. An STBC transmitting four symbols across four antennas in eight time slots will have a rate of 0.5, while an STBC transmitting two symbols across two antennas in two time slots will have a rate of 1.

Due to construction constraints, no orthogonal rate 1 codes exist for systems with more than two antennas. Tarokh, Jafarkhani and Calderbank [33] showed that generalised orthogonal STBC designs exist that achieve rate 0.5 for any number of antennas. In the same paper they also presented rate 0.75 orthogonal STBCs for three and four transmitting antennas.

Quasi-orthogonal STBCs sacrifice full orthogonality to achieve higher rates [34]. Each column only needs to be orthogonal to a subset of the other columns rather than all columns. Several quasi-orthogonal STBCs have been developed, balancing diversity, rate and decoding complexity [34–36].

A noteworthy STBC for a 2×2 antenna system was proposed by Siavash Alamouti in [28]. It is of particular interest since it achieves orthogonality while maintaining a rate of 1, transmitting two symbols in every two time slots. Since the code is orthogonal, the diversity of the Alamouti scheme is $n_T n_R = 4$, i.e. full diversity is achieved. The structure of the Alamouti STBC is given in table 2.2.

TABLE 2.2: Alamouti encoding scheme

	t_1	t_2
TX Antenna 1	x_1	$-x_2^*$
TX Antenna 2	x_2	x_1^*

The transmitted symbols pass through the channel and are received by two antennas, as shown in table 2.3.

TABLE 2.3: Received symbol notation

	t_1	t_2
RX Antenna 1	r_1	r_3
RX Antenna 2	r_2	r_4

Combining the definition for the channel matrix

$$\mathbf{H} = \begin{bmatrix} h_{11} & h_{12} \\ h_{21} & h_{22} \end{bmatrix} ,$$

and the equation for the received vector $\mathbf{r} = \mathbf{Hx} + \mathbf{n}$, the expressions for the individual received symbols can be derived:

$$r_1 = h_{11}x_1 + h_{12}x_2 + n_1 , \tag{2.20}$$

$$r_2 = h_{21}x_1 + h_{22}x_2 + n_2 , \tag{2.21}$$

$$r_3 = -h_{11}x_2^* + h_{12}x_1^* + n_3 , \text{ and} \tag{2.22}$$

$$r_4 = -h_{21}x_2^* + h_{22}x_1^* + n_4 . \tag{2.23}$$

The Alamouti scheme uses maximal ratio combining (MRC) to generate the decision statistics y_i for the recovered symbols. MRC generates a decision statistic by summing all samples multiplied by the complex conjugate of the relevant entry from the channel matrix. This technique causes the channel paths with the least attenuation to have the greatest contribution to the decision statistic. The decision statistics are thus

$$y_1 = h_{11}^* r_1 + h_{21}^* r_2 + h_{12} r_3^* + h_{22} r_4^* \text{ , and} \tag{2.24}$$

$$y_2 = h_{12}^* r_1 + h_{22}^* r_2 - h_{11} r_3^* - h_{21} r_4^* \text{ .} \tag{2.25}$$

Substituting in equations 2.20-2.23, the following expressions are obtained:

$$y_1 = \sum_{i,j} |h_{ij}|^2 x_1 + h_{11}^* n_1 + h_{21}^* n_2 + h_{12} n_3^* + h_{22} n_4^* \text{ , and} \tag{2.26}$$

$$y_2 = \sum_{i,j} |h_{ij}|^2 x_2 + h_{12}^* n_1 + h_{22}^* n_2 - h_{11} n_3^* - h_{21} n_4^* \text{ .} \tag{2.27}$$

The decision statistics are then passed to a maximum likelihood (ML) decoder. The ML decoder selects the output symbol $y_1 = s_a$ if

$$\left(\sum_{i,j} |h_{ij}|^2 - 1 \right) |s_a|^2 + d^2(y_1, s_a) \leq \left(\sum_{i,j} |h_{ij}|^2 - 1 \right) |s_b| + d^2(y_1, s_b) \qquad \forall\, a \neq b \text{ ,} \tag{2.28}$$

where $d^2(a, b)$ is the square of the Euclidean distance between points a and b. The output symbol y_2 is selected by the ML decoder in the same way.

This concludes the discussion on MIMO transmission schemes and the associated decoding methods. The following section describes channel coding techniques for correcting errors produced by the MIMO decoding.

2.3 Reed-Solomon error correcting codes

2.3.1 Introduction

When transmitting information across a noisy channel, some corruption of the information may occur. Channel coding involves transmitting additional symbols, called parity,

which allow the receiver to detect or even correct the errors. If errors are simply detected, the receiver would have to request that the information be retransmitted. Error correction, on the other hand, allows the receiver to reconstruct the original information without any retransmission.

If the number of parity symbols is given as p, a code can reliably correct at most $\frac{p}{2}$ errors, while it can detect at most p errors [37]. Most codes, however, do not achieve these bounds.

Reed-Solomon (RS) codes are class of non-binary error correcting codes developed by Irving Reed and Gustave Solomon in 1960 [5]. They are one of the few types of codes to achieve these bounds. Since it is a non-binary code, each symbol in the codeword consists of more than one bit. RS codes have many applications ranging from optical and magnetic storage to wired and wireless communication [38, 39].

2.3.1.1 Algebra background

In order to discuss construction and decoding of Reed-Solomon codes, some concepts relating to the algebra of finite fields must first be defined.

Definition 2.1. A *field* $\mathbb{F}$ is a set of elements on which the operations addition, multiplication and their inverses work in a way analagous to the way it works for real numbers. Additionally, the field must have the following properties for both the addition and multiplication operators:

1. It must be closed under the operation: for $a, b \in \mathbb{F}$, $a + b \in \mathbb{F}$ and $a \cdot b \in \mathbb{F}$.
2. It must have an additive and multiplicative identity, denoted 0 and 1 respectively: $a + 0 = a$; $a \cdot 1 = a$.
3. Every element must have an additive inverse, and every element other than 0 must have a multiplicative inverse: There exists b such that $a + b = 0 \,\forall\, a \in \mathbb{F}$ and there exists c such that $a \cdot c = 1 \,\forall\, a \in \mathbb{F}, a \neq 0$.
4. Operations must be associative: $(a+b)+c = a+(b+c)$ and $(ab)c = a(bc) \;\forall\; a, b, c \in \mathbb{F}$ [37].

The set of real numbers ($\mathbb{R}$) is thus a field, but integers ($\mathbb{Z}$) is not, since not all elements have a multiplicative inverse.

Definition 2.2. A *finite field* or *Galois field*, denoted $\mathbb{F}_{p^m}$, is a field which contains a finite number of elements [37].

The number of elements in a Galois field is called the *cardinality*, and is of the form p^m, where p is prime and m is a natural number. A Galois field of order p^m can also be represented as GF(p^m). When $m = 1$, the field is called a prime field. All multiplication and addition in a prime field is performed by applying the modulo p operation.

For prime extension fields, where $m > 1$, elements are represented as polynomials of degree $m - 1$ with coefficients from GF(p). The value of the polynomial is defined as $f(x)|_{x=p}$. Addition of polynomials is performed by adding coefficients in GF(p).

Definition 2.3. An *irreducible polynomial* is a polynomial with coefficients in $\mathbb{F}$ which cannot be factorised into two or more non-constant polynomials with coefficients which are also in $\mathbb{F}$ [37].

A trivial example of an irreducible polynomial in the field of real numbers is $f(x) = x^2+1$. Although it can be factorised into $(x + i)(x - i)$, the coefficients of the factors are not in the field of real numbers.

Definition 2.4. A *primitive polynomial* $P(x)$ of degree m is an irreducible polynomial which satisfies the condition that the smallest integer for which $P(x)$ divides $x^n + 1$ is $n = p^m - 1$ [37].

When constructing a Galois field $\mathbb{F}_{p^m}$, a primitive polynomial $P(x)$ of degree m is selected. Polynomial multiplication is performed modulo $P(x)$. For example, if

$$P(x) = x^3 + x + 1$$

in the field $\mathbb{F}_{2^3}$ then

$$x \times x^2 = x^3 \bmod P(x) = x + 1 \ .$$

For simpler notation when performing multiplication, elements of the field can be represented as powers of α, where $\alpha = p$. Multiplication can then be performed by adding exponents of α modulo p^m.

2.3.1.2 Error control coding fundamentals

Error correcting codes fall into two categories: block codes, which have a fixed codeword length, and convolutional codes, which operate on a continuous stream of data. Block codes encode messages of length k symbols into codewords consisting of n symbols, and thus have a rate of $R = \frac{k}{n}$. Convolutional encoders also produce n symbols for every k symbols in the input stream, but the output is a continuous stream rather than a series of codewords.

The symbols which make up a code are drawn from an alphabet $\mathcal{A}$, which has cardinality q. In the case where the alphabet is a Galois field, $\mathcal{A} = \mathrm{GF}(p^m)$ and $q = p^m$. In addition to defining a code as having a block or convolutional structure, it can also be classified according to the cardinality of the alphabet. Binary codes use an alphabet with a cardinality of two, since the only elements in the alphabet are 0 and 1. Alphabets of non-binary codes have higher cardinalities, defined by the field which is used for the code.

An important property of an error correcting code is the minimum distance of the code, as this defines the error correcting capability of the code.

Definition 2.5. The Hamming weight of a vector is the number of non-zero entries in that vector [37].

Definition 2.6. The Hamming distance between two vectors $\boldsymbol{u}$ and $\boldsymbol{v}$, denoted $d(\boldsymbol{u}, \boldsymbol{v})$ is the number of positions in which $\boldsymbol{u}$ and $\boldsymbol{v}$ differ [37].

Definition 2.7. The minimum distance, denoted $d_{\min}$, is the minimum Hamming distance between any two codewords of a code C.

$$d_{\min} = \min\{d(\boldsymbol{u}, \boldsymbol{v}) : \boldsymbol{u}, \boldsymbol{v} \in C, \boldsymbol{u} \neq \boldsymbol{v}\} \tag{2.29}$$

[37]

The minimum distance of a code defines the number of errors that the code can reliably detect or correct. Since no codewords differ in fewer than $d_{\min}$ locations, all error patterns of weight no larger than $d_{\min} - 1$ will result in an invalid codeword. A code with minimum distance $d_{\min}$ is thus capable of reliably detecting up to $d_{\min} - 1$ errors in a codeword.

The upper bound on the minimum distance of a code is given by the Singleton bound [4]:

Definition 2.8. The Singleton bound states that a q-ary code of length n and minimum distance $d_{\min}$ can have at most A_q codewords, where

$$A_q \leq q^{n-d_{\min}+1} \; . \tag{2.30}$$

The number of codewords in a code is also limited by k, the number of information symbols in a code, since $A_q \leq q^k$. The upper bound for the minimum distance of an (n, k) code can thus be determined as follows:

$$q^k \leq q^{n-d_{\min}+1} \tag{2.31}$$

$$\therefore \quad k \leq n - d_{\min} + 1 \tag{2.32}$$

$$\therefore \quad d_{\min} \leq n - k + 1 \; . \tag{2.33}$$

Codes that achieve this bound with equality, i.e. $d_{\min} = n - k + 1$, are called Maximum Distance Separable (MDS). Some trivial codes achieve this bound, such as the (n, n) code, which is essentially an uncoded system. A non trivial class of codes that are MDS are Reed-Solomon codes [5]. Since RS codes can correct the largest number of errors for a given rate code, they are well suited to this research.

2.3.2 Reed-Solomon encoding

The original encoding technique proposed by Reed and Solomon was to consider the message to be the k coefficients of a polynomial in $\mathbb{F}_q$ with degree $k - 1$.

$$m(x) = m_1 + m_2 x + \cdots + m_k x^{k-1} \qquad m_i \in \mathbb{F}_q \tag{2.34}$$

The codeword is generated by sampling the message polynomial $m(x)$ at $n = q - 1$ points:

$$\mathbf{c} = \big(m(x_1),\, m(x_2),\, \cdots,\, m(x_n)\big) \; . \tag{2.35}$$

This structure allows algebraic decoders to recover the message polynomial by means of interpolation. It is generally preferable, however, to use a systematic code so that the codeword contains a copy of the message. In the event of a decoding failure, the decoder can return the message portion as it was received. Although some of the message symbols may contain errors, this avoids losing the entire message.

One way of achieving a systematic code structure is to find a polynomial $p(x)$ such that

$$\big(p(x_1),\, p(x_2), \cdots,\, p(x_k)\big) = (m_1,\, m_2, \cdots,\, m_k)\,,$$

where m_i is the ith message symbol. Encoding $p(x)$ thus yields a systematic codeword which contains m. An algebraic decoder will, however, produce $p(x)$. This polynomial must then be re-encoded to produce the original message symbols.

2.3.3 Reed-Solomon decoding

Reed-Solomon decoders can be divided into two categories based on the type of input: hard decision decoders and soft decision decoders. The difference between the two is that soft decision decoders take the reliability of each symbol into account whereas hard decision decoders do not.

2.3.3.1 Hard decision

The input to a hard decision decoding algorithm is a vector of length n with elements taken from $\mathbb{F}_{n+1}$. By definition, a hard decision decoding algorithm can correct $t = \left\lfloor \frac{d_{\min}-1}{2} \right\rfloor$ errors. Since no codewords are within a Hamming distance of $d_{\min}$ of each other, at most one codeword will be within a distance of t of any received vector. When more than t errors occur, one of two things can happen: either a non-causal codeword is within a distance of t from the received vector, or no codewords are within this distance. These conditions are known as a decoding error and decoding failure respectively. Since Reed-Solomon codes have the property that $d_{\min} = n - k + 1$, they can correct up to $t = \lfloor \frac{n-k}{2} \rfloor$ errors.

Hard decision decoding algorithms such as Berlekamp-Massey and the Euclidean decoding algorithm only differ in complexity, not decoding performance [37]. As such,

the particular implementation of hard decision decoding is not of particular interest to this research. The MATLAB implementation of the Berlekamp-Massey decoding algorithm [40] is used for hard decision simulations.

2.3.3.2 Soft decision

When hard decision decoding is used, the demodulator provides no reliability information to the decoder. All input values to the demodulator are essentially quantised to the nearest constellation point. Quantisation converts analogue values to digital values, which causes loss of information. To visualise this loss of information, compare two received points on a constellation diagram, as depicted in figure 2.4. The first point, x_1 is located very close to constellation point 13, while the second point is near the decision boundary between 13, 15, 9 and 11.

Intuitively, the likelihood that the causal symbol for x_1 was 13 is very high. The likelihood that the causal symbol for x_2 was 13, however, is only marginally greater than the likelihood that it was 9, 15 or 11. A hard decision approach would quantize both points to 13, despite the very low likelihood that $x_2 = 13$.

Soft decision decoding makes use of the likelihood information as part of the decoding process. When attempting to construct a codeword, the decoder can thus place more emphasis on reliable symbols while marginalising or even ignoring unreliable symbols. The Guruswami-Sudan (GS) algorithm [41] with the Koetter-Vardy (KV) extension [42] is a soft decision decoding algorithm which uses symbol reliability information as input and produces a list of potential messages.

2.3.3.3 Guruswami-Sudan algorithm

Conventional decoding algorithms such as the Berlekamp-Massey algorithm [43] produce a single output message or codeword per received vector. This is an effective approach to decoding when the number of errors $e < \frac{d_{\min}}{2}$, as it is within the error correcting capability of the code. There is thus only one codeword within a Hamming distance of e from the received vector. When $e \geq \frac{d_{\min}}{2}$, however, there can be multiple codewords within a Hamming distance of e. To recover the original message it is thus necessary for the decoder to return more than one output - this is known as list decoding.

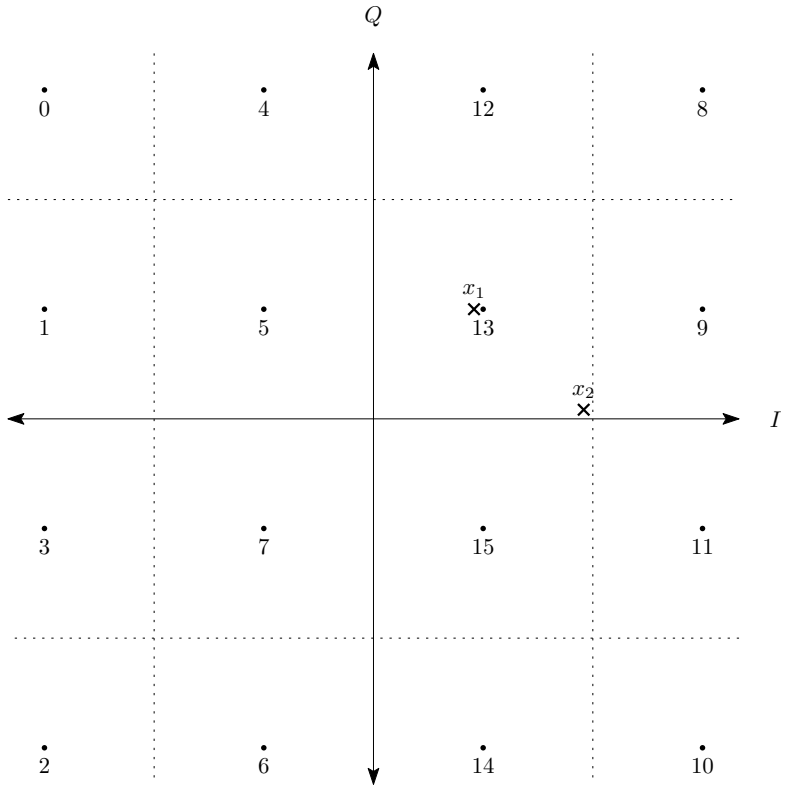


FIGURE 2.4: 16-QAM constellation with one reliable and one unreliable symbol

The Guruswami-Sudan algorithm[1] [41] is a list decoding algorithm. The approach used in the GS algorithm is to consider the received vector as a set of noisy samples of a polynomial. The algorithm then generates a bivariate polynomial $Q(x, y)$ by interpolating the samples. Finally the bivariate polynomial is factorised into factors of the form $(y - f_i(x))$, where $f_i(x)$ are the canditate message polynomials in the list. If $f_i(x) = m(x)$ for some value of i, decoding was performed successfully.

The GS algorithm forms part of a flow of information, starting at the demodulator and ending when a single output message has been calculated. This is represented in figure 2.5.

The first step in the GS algorithm is to select the sample points to be used for interpolating the polynomial. The codeword $\mathbf{c}$ was generated by evaluating the message $m(x)$ at n points $(\alpha_1, \alpha_2, \cdots, \alpha_n)$. Given a bivariate polynomial $Q(x, y)$ which has y-roots of the form $y = m(x)$, $Q(x, y)$ will thus have (x, y) roots at (α_i, c_i).

[1]The tutorial paper by McEliece [44] was of invaluable help when implementing the GS algorithm. The theorems and definitions presented in this section are based on the same paper.

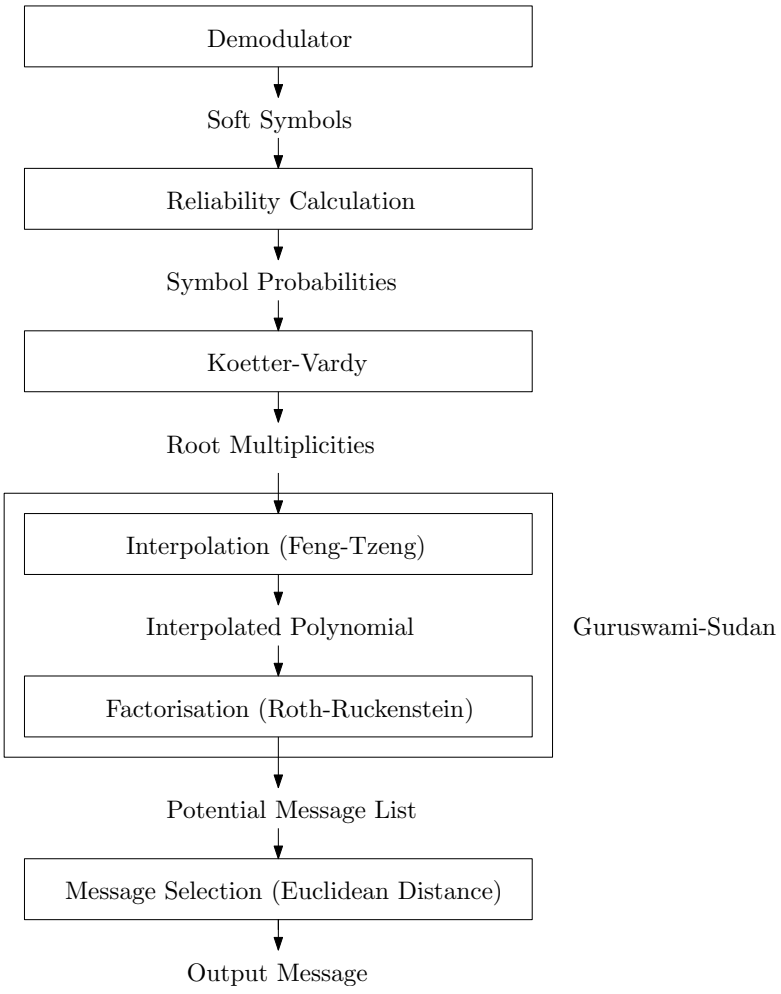


FIGURE 2.5: Flow diagram from demodulator output to final output message

The analogue received vector $\mathbf{r}$ must be converted into y values to be passed to the interpolation algorithm. A simple approach is to use a hard decision demodulator to demodulate $\mathbf{r}$ into $(\beta_1, \beta_2, \cdots, \beta_n)$, where β_i is the symbol in $\mathbb{F}$ which is closest to r_i. An advanced technique which also passes the soft information to the decoder is discussed in section 2.3.3.4.

Interpolation

In order to define the nature of the interpolated polynomial, it is necessary to first define the degree of a bivariate polynomial.

Definition 2.9. The (u, v) weighted degree of a monomial $x^i y^j$ is defined as $ui + vj$.

The sampled points which must be interpolated are of the form (α_i, β_i). The interpolation algorithm constructs a polynomial $Q(x, y)$ of minimum $(1, k-1)$ degree with

zeroes at ($x = \alpha_i$, $y = \beta_i$). In order to improve the accuracy of the interpolation, the multiplicity of each of the zeroes can be increased to be greater than one. A zero of multiplicity m will thus mean that the curve Q passes through that point m times.

Guruswami and Sudan demonstrate in [41] that the error correcting capability t is a monotonically increasing function of m, with some limit t_{GS}. The value of m that achieves t_{GS} is dependent on the codeword length n and the message length k, but the exact relationship is not stated. The error correcting bound is given as

$$t_{GS} = n - 1 - \left\lfloor \sqrt{(k-1)n} \right\rfloor \ . \tag{2.36}$$

The difference between this error correcting bound and the hard decision decoding bound of $\left\lfloor \frac{n-k}{2} \right\rfloor$ is visualised in figure 2.6.

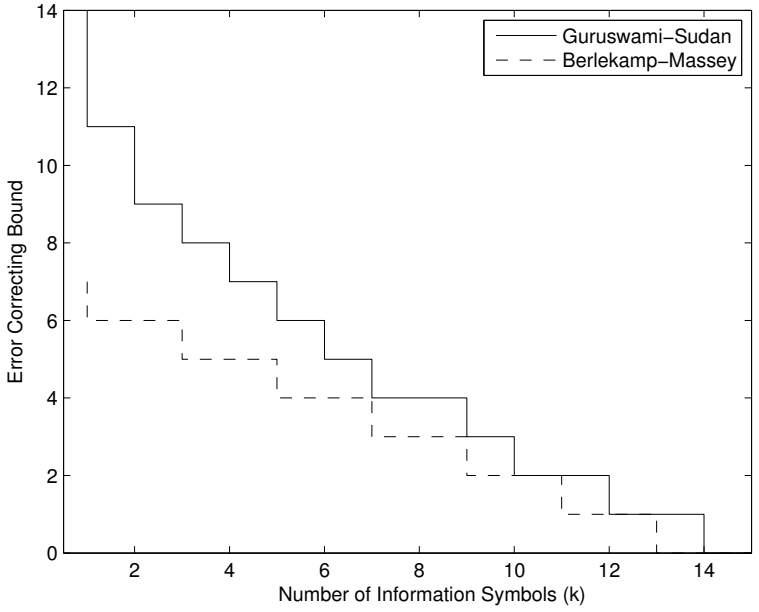


FIGURE 2.6: Comparison of the error correcting bounds for the Guruswami-Sudan and Berlekamp-Massey algorithms. Codeword length $n = 15$.

Using the same multiplicity m for all the received symbols is, however, not optimal. Certain symbols may have lower reliability and the interpolated polynomial need not pass through these points as many times. By optimally selecting the multiplicities for each symbol, performance exceeding the bound given in equation 2.36 can be achieved. One algorithm for selecting multiplicities is the Koetter-Vardy algorithm [42], which is discussed in section 2.3.3.4.

When using the same multiplicity for all symbols, the interpolated polynomial $Q(x, y)$ has y-degree equal to m. This means that there are m factors of the form $(y - f_i(x))$ where the degree of $f_i(x)$ is at most $k - 1$. The polynomials $f_i(x)$ where $0 \leq i \leq m$ are the recovered messages, of which one of them is ideally equal to $m(x)$.

In order to interpolate a polynomial, the constraints which define the polynomial have to be stipulated. If $(x = \alpha_i,\ y = \beta_i)$ is a root of $Q(x, y)$, it is clear that $Q(\alpha_i, \beta_i) = 0$. If the root has multiplicity m, the curve described by $Q(x, y)$ passes through (α_i, β_i) a total of m times. It is thus not sufficient to only require that $Q(\alpha_i, \beta_i) = 0$.

For a single variable polynomial with a root $x = \alpha$ of multiplicity m the first $m - 1$ derivatives also satisfy the equation

$$\left.\frac{d^i y}{dx^i}\right|_{x=\alpha} = 0\ . \tag{2.37}$$

An example using real numbers was developed to illustrate the relationship between higher multiplicity roots and derivatives. The equation $y = (x + 2)^3$ in $\mathbb{R}$ has the root $x = -2$ with a multiplicity of 3. Figure 2.7 shows y and the first two derivatives of y with respect to x. It is clear from the graph that $y = \frac{dy}{dx} = \frac{d^2y}{dx^2} = 0$ only where $x = -2$. All higher order derivatives are constant and equal to zero. For a root of multiplicity 3, the zeroth, first and second derivatives are equal to zero at $x = -2$.

The proof for the constraint in equation 2.37 is based on two theorems by Hasse [45]. Theorem 2.10 handles the single variable polynomial case, while theorem 2.11 extends similar logic to the bivariate polynomial.

Theorem 2.10. *If $Q(x) = \sum_i a_i x^i \in \mathbb{F}[x]$, then for any $\alpha \in \mathbb{F}$, we have*

$$Q(x + \alpha) = \sum_r Q_r(\alpha) x^r\ , \tag{2.38}$$

where

$$Q_r(x) = \sum_i \binom{i}{r} a_i x^{i-r}\ , \tag{2.39}$$

which is the rth Hasse derivative of $Q(x)$ (from [44]).

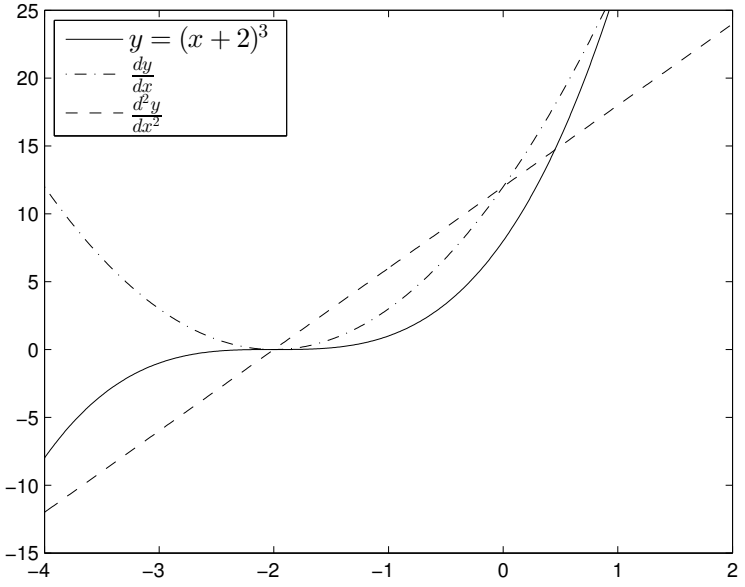


FIGURE 2.7: Relationship between root multiplicities and derivatives

Theorem 2.11. *Let* $Q(x,y) = \sum_{i,j} a_{i,j} x^i y^j \in \mathbb{F}[x,y]$ *where* $\mathbb{F}$ *is a finite field. For any* $(\alpha,\beta) \in F^2$,

$$Q(x+\alpha,\ y+\beta) = \sum_{r,s} Q_{r,s}(\alpha,\beta) x^r y^s \ , \tag{2.40}$$

where

$$Q_{r,s}(x,y) = \sum_{i,j} \binom{i}{r}\binom{j}{s} a_{i,j} x^{i-r} y^{j-s} \ . \tag{2.41}$$

Note that the binomial distribution must be performed modulo p, where p is the characteristic of the field $\mathbb{F}$ *(from [44]).*

Corollary 2.12. *The polynomial* $Q(x,y)$ *has a zero of multiplicity* m *at* (α,β) *if and only if*

$$Q_{r,s}(\alpha,\beta) = 0 \quad \forall\, r,s \quad \textit{such that} \quad 0 \le r+s < m \textit{ (from [44]).} \tag{2.42}$$

Corollary 2.12 thus defines the constraints that the interpolated $Q(x,y)$ has to satisfy.

In order to express the bivariate polynomial $Q(x,y)$ in a uniform manner, it is necessary to define the order in which the monomial terms are arranged.

Definition 2.13. (u,v)-revlex order is an ordering of monomials in ascending (u,v) weighted degree. Where two monomials have equal (u,v) degree, the monomial with the lower $(0,1)$ degree comes first in the revlex ordering.

In order to achieve a list length of at most L, the polynomial $Q(x, y)$ should be of the form $(y - \widehat{m}_1(x))(y - \widehat{m}_2(x)) \cdots (y - \widehat{m}_L(x))$. Since $\widehat{m}_i(x)$ consists of monomials up to x^{k-1}, each factor of $Q(x, y)$ consists of the monomials up to and including y in $(1, k-1)$-revlex order. $Q(x, y)$ thus consists of the monomials up to and including y^L in $(1, k-1)$-revlex order.

Example 2.1. *Consider a message of length 3 in* GF(8)*, using a primitive root satisfying* $\alpha^3 = \alpha + 1$*. Since* $k = 3$*, the monomial order used is* $(1, 2)$*-revlex.* $Q(x, y)$ *will be of the form*

$$a_1 + a_2x + a_3x^2 + a_4y + a_5x^3 + a_6xy + a_7x^4 + a_8x^2y + a_9y^2 \ . \tag{2.43}$$

Suppose that the polynomial $Q(x, y)$ *to be interpolated has* (x, y) *roots* $(\alpha^2, 1)$*,* $(1, \alpha^3)$*,* (α^3, α^2)*,* (α^4, α^6)*,* (α^5, α^6)*,* (α, α^5) *and* (α^6, α^5)*, and that all roots have multiplicity* 1*, except for* $(\alpha^2, 1)$ *which has multiplicity* 2*. The constraints imposed by roots with multiplicity* 1 *are that* $Q(x, y)|_{(\alpha_i, \beta_i)} = 0$*. The root with multiplicity* 2 *imposes the constraints* $Q(\alpha^2, 1) = Q_{0,1}(\alpha^2, 1) = Q_{1,0}(\alpha^2, 1) = 0$*. The basic form of* Q *and its mixed partial derivatives is shown in equation 2.44.*

$$\begin{array}{lcccccccccccccccccc}
Q_{0,0}(x,y) & = & 1 & + & x & + & x^2 & + & y & + & x^3 & + & xy & + & x^4 & + & x^2y & + & y^2 \\
Q_{1,0}(x,y) & = & & & 1 & & & & & + & x^2 & + & y & & & & & \\
Q_{0,1}(x,y) & = & & & & & & & 1 & & & + & x & & & + & x^2 & &
\end{array} \tag{2.44}$$

Substituting in the values for the roots gives

	1	x	x^2	y	x^3	xy	x^4	x^2y	y^2
$Q_{0,0}(\alpha^2, 1)$	1	α^2	α^4	1	α^6	α^2	α	α^4	1
$Q_{0,1}(\alpha^2, 1)$	0	0	0	1	0	α^2	0	α^4	0
$Q_{1,0}(\alpha^2, 1)$	0	1	0	0	α^4	1	0	0	0
$Q_{0,0}(1, \alpha^3)$	1	1	1	α^3	1	α^3	1	α^3	α^6
$Q_{0,0}(\alpha^3, \alpha^2)$	1	α^3	α^6	α^2	α^2	α^5	α^5	α	α^4
$Q_{0,0}(\alpha^4, \alpha^6)$	1	α^4	α	α^6	α^5	α^3	α^2	1	α^5
$Q_{0,0}(\alpha^5, \alpha^6)$	1	α^5	α^3	α^6	α	α^4	α^6	α^2	α^5
$Q_{0,0}(\alpha, \alpha^5)$	1	α	α^2	α^5	α^3	α^6	α^4	1	α^3
$Q_{0,0}(\alpha^6, \alpha^5)$	1	α^6	α^5	α^5	α^4	α^4	α^3	α^3	α^3

. (2.45)

Equation 2.45 is the constraint matrix $\mathbf{A}$, which forms the input to the Feng-Tzeng interpolation algorithm. The Feng-Tzeng (FT) algorithm [46] has complexity $\mathcal{O}(m^3)$ and is detailed in algorithm 2. The purpose of the Feng-Tzeng algorithm is to find the largest L for which the first L columns of $\mathbf{A}$ are linearly independent. The output of the FT algorithm is a length $L+1$ vector $\mathbf{c_s}$ for which

$$\sum_{i=1}^{L+1} c_{s_i} \mathbf{A^{(i)}} = 0 \ ,$$

where $\mathbf{A^{(i)}}$ denotes the ith column of $\mathbf{A}$. This vector is the list of coefficients of the interpolated polynomial $Q(x, y)$ in $(1, k-1)$-revlex order.

Algorithm 2: Feng-Tzeng Interpolation Algorithm (adapted from [44])

Input: Constraint matrix $\mathbf{A}$ with dimensions $v \times w$
Output: $\mathbf{c_s}$, the coefficients of $Q(x, y)$ in $(1, k-1)$-revlex order

```
s = 0
repeat
    s = s + 1
    r = 0
    b = [b_1, b_2, ..., b_w],   b_i = { 1  if i = s
                                      { 0  if i ≠ s
    columnblocked = false
    repeat
        r = r + 1
        Δ = a_r . b
        if Δ ≠ 0 then
            if there is a u < s such that ρ_u == r then
                b = b − (Δ/δ_u) c_u
            else
                ρ_s = r
                δ_s = Δ
                c_s = b
                columnblocked = true
            end
        end
    until r ≥ v or columnblocked == true
until columnblocked == false
c_s = b
```

The steps in the Feng-Tzeng algorithm are explained as follows:

3. The outer loop counter s specifies which row of the output matrix is being generated.

4. The inner loop counter r tracks the current row of $\mathbf{A}$

5. $\mathbf{b}$, a starting estimate for $\mathbf{c_s}$, is initialised to be orthogonal to all previous values of $\mathbf{c}$

6. Both loops terminate based on whether a $\mathbf{b}$ has been found which is orthogonal to a previously unused row of $\mathbf{A}$. It is initially false.

8. The inner loop counter, which points to rows of $\mathbf{A}$, is incremented

9. Δ checks whether $\mathbf{b}$ is orthogonal to the rth row of $\mathbf{A}$

12. If the vectors were not orthogonal and the inner loop had previously terminated on the current row, modify $\mathbf{b}$ so that it becomes orthogonal to $\mathbf{a_r}$

14. If the inner loop had not previously terminated on the current row, save the row number, Δ and $\mathbf{b}$.

The following example demonstrates the functioning of the Feng-Tzeng algorithm.

Example 2.2. *Using the constraint matrix* $\mathbf{A}$ *from example 2.1, the Feng-Tzeng algorithm generates* $\mathbf{C}$*, with rows* $\mathbf{c_s}$*.*

$$\mathbf{C} = \begin{pmatrix} 1 & 0 & 0 & 0 & 0 & 0 & 0 & 0 & 0 \\ \alpha^2 & 1 & 0 & 0 & 0 & 0 & 0 & 0 & 0 \\ \alpha^4 & 0 & 1 & 0 & 0 & 0 & 0 & 0 & 0 \\ 1 & 0 & 0 & 1 & 0 & 0 & 0 & 0 & 0 \\ \alpha^4 & \alpha^4 & 1 & 0 & 1 & 0 & 0 & 0 & 0 \\ 0 & 0 & \alpha^5 & \alpha^2 & \alpha^3 & 1 & 0 & 0 & 0 \\ 1 & \alpha^5 & \alpha^2 & \alpha^4 & \alpha^6 & \alpha^2 & 1 & 0 & 0 \\ 0 & 0 & \alpha^2 & \alpha^6 & \alpha^4 & \alpha & \alpha^3 & 1 & 0 \\ 0 & 0 & \alpha^2 & \alpha^6 & \alpha^6 & \alpha^3 & \alpha^2 & \alpha^4 & 1 \end{pmatrix}$$

The final row of $\mathbf{C}$ *comprises the coefficients of* $Q(x, y)$ *in* $(1, 2)$*-revlex order, thus the interpolated polynomial is*

$$Q(x, y) = \alpha^2 x^2 + \alpha^6 y + \alpha^6 x^3 + \alpha^3 xy + \alpha^2 x^4 + \alpha^4 x^2 y + y^2 \, .$$

Factorisation

Once the bivariate polynomial $Q(x, y)$ has been constructed it must be factorised to isolate the factors $\prod_i \big(y - \widehat{m}_i(x)\big)$. The Roth-Ruckenstein (RR) algorithm performs factorisation by recursively finding coefficients of potential factors. It is described in algorithm 3. The approach used is to extract one coefficient of $\widehat{m}_i(x)$ at a time, recursing to create a tree where the branches are the coefficients. The method used for extracting the coefficients is explained by the following two theorems.

Definition 2.14. If $x^m \mid Q(x, y)$ but $x^{m+1} \nmid Q(x, y)$,

$$\langle\langle Q(x, y)\rangle\rangle \triangleq \frac{Q(x, y)}{x^m} .$$

Theorem 2.15. *If* $(y - f(x)) \mid Q(x, y)$ *then* $y = f(0)$ *is a root of the equation*

$$\langle\langle Q(0, y)\rangle\rangle = 0 .$$

Proof. From the definition of $\langle\langle\cdot\rangle\rangle$, $Q(x, y) = x^m\langle\langle Q(x, y)\rangle\rangle$ for some $m \geq 0$. If $\big(y-f(x)\big)$ divides $Q(x, y)$ then it will also divide $\langle\langle Q(x, y)\rangle\rangle$, and thus

$$\langle\langle Q(x, y)\rangle\rangle = \big(y - f(x)\big)T(x, y)$$

for some polynomial $T(x, y)$. Thus, $y = f(0)$ is a root of the equation $\langle\langle Q(0, y)\rangle\rangle = 0$ (from [44]). □

Theorem 2.15 is sufficient for extracting the constant term, but an induction based approach is necessary to extract the rest of the coefficients. The initial conditions are [44]

$$f_0(x) = f(x) \qquad \text{and} \tag{2.46}$$

$$Q_0(x, y) = \langle\langle Q(x, y)\rangle\rangle . \tag{2.47}$$

Induction is done as follows for $i \geq 1$:

$$f_i(x) = \big(f_{i-1}(x) - f_{i-1}(0)\big)/x \;=\; a_i + \cdots + a_v x^{v-i} \tag{2.48}$$

$$T_i(x, y) = Q_{i-1}(x, xy + a_{i-1}) \tag{2.49}$$

$$Q_i(x, y) = \langle\langle T_i(x, y)\rangle\rangle . \tag{2.50}$$

Theorem 2.16. *Given $f(x)$ of the form $a_0+a_1x+\cdots+a_vx^v$, $Q(x,y)$ and the definitions in equations 2.46 to 2.50. For any $i \geq 1$, $\big(y - f(x)\big) \mid Q(x,y)$ iff $\big(y - f_i(x)\big) \mid Q_i(x,y)$*

Proof. The proof consists of two parts: proving that for $i \geq 1$, $\big(y - f(x)\big) \mid Q(x,y) \quad \rightarrow \big(y - f_i(x)\big) \mid Q_i(x,y)$ and vice versa.

First, assume $\big(y - f_i(x)\big) \mid Q_i(x,y)$. Since $T_i(x,y) = x^m Q_i(x,y)$,

$$\begin{aligned} &\big(y - f_i(x)\big) \mid T_i(x,y) \qquad \text{and} \\ &\big(y - f_i(x)\big) \mid Q_{i-1}(x, xy + a_{i-1}) \ . \end{aligned}$$

Therefore, for some $U(x,y)$,

$$Q_{i-1}(x, xy + a_{i-1}) = \big(y - f(x)\big)U(x,y) \ .$$

Substituting in $y = \frac{y - a_{i-1}}{x}$,

$$Q_{i-1}(x,y) = \left(\frac{y - a_{i-1}}{x} - f(x)\right) U\left(x, \frac{y - a_{i-1}}{x}\right) \ .$$

Multiplying by a sufficiently large power of x

$$x^L Q_{i-1}(x,y) = \big(y - f_{i-1}(x)\big)V(x,y)$$

for some polynomial $V(x,y)$. Thus $\big(y - f_{i-1}(x)\big) \mid Q_{i-1}(x,y)$, which constitutes the first part of the proof.

For the second part of the proof, assume $\big(y - f_{i-1}(x)\big) \mid Q_{i-1}(x,y)$. Then

$$Q_{i-1}(x,y) = \big(y - f_{i-1}(x)\big)U(x,y)$$

for some $U(x,y)$. Substituting in the definition of $T_i(x,y)$ from equation 2.49

$$\begin{aligned} T_i(x,y) &= \big(xy + a_{i-1} - f_{i-1}(x)\big)U(x, xy + a_{i-1}) \\ &= x\big(y - f_i(x)\big)U(x, xy + a_{i-1}) \ . \end{aligned}$$

This proves that $\big(y - f_i(x)\big) \mid T_i(x,y)$, and thus $\big(y - f_i(x)\big) \mid Q_i(x,y)$ as well (from [44]).

□

The corollary to this theorem allows extracting coefficients one at a time

Corollary 2.17. *If* $\big(y - f(x)\big) \mid Q(x, y)$ *then* $y = a_i$ *is a root of the equation*

$$Q_i(0, y) = 0 \quad \forall \quad 0 \leq i \leq v \; .$$

Proof. By Theorem 2.16, $\big(y - f_i(x)\big) \mid Q_i(x, y)$ for all $i \geq 0$. Substituting $x = 0$ yields the required result, since $f_i(0) = a_i$ (from [44]). □

Algorithm 3: Roth-Ruckenstein Factorisation Algorithm (adapted from [44])

Input: $Q(x, y)$, the interpolated polynomial, and D, the desired degree of $\widehat{m}_i(x)$
Output: $\widehat{m}_i(x)$, the potential decoded messages
Initialise: $\pi_1 = 0,\ d_1 = -1,\ Q_1(x, y) = Q(x, y)\ t = 2; u = 1$
begin DepthFirstSearch(u)
3 | **if** $Q(x, 0) == 0$ **then**
 | | Output $\widehat{m}_{[u]}(x)$
5 | **else if** $d_u < D$ **then**
6 | | $R = \text{Roots}\big(Q_u(0, y)\big)$
 | | **for** $\alpha \in R$ **do**
8 | | | $v = t,\ t = t + 1$
9 | | | $\pi_v = u,\ d_v = d_u + 1,\ \text{coeff}_v = \alpha$
10 | | | $Q_v(x, y) = \langle\langle Q_u(x, xy + \alpha)\rangle\rangle$
11 | | | DepthFirstSearch(v)
 | | **end**
 | **end**
end

The notation used in algorithm 3 is as follows:

- π_u – the parent node of node u
- d_u – the degree of node u, i.e. the distance to the root node
- coeff_u – the polynomial coefficient represented by node u
- $\widehat{m}_{[u]}(x)$ – the polynomial coefficients $\text{coeff}_u x^{d_u} + \text{coeff}_{\pi_u} x^{d_{\pi_u}} + \cdots$

The algorithm generates a tree of coefficients – the path from the root to the tip of the tree is the list of coefficients in $\widehat{m}(x)$. Line 3 is the terminating condition in the event that a valid factor has been found. The condition in line 5 causes the algorithm to continue until the degree of the factorised polynomial is D. The tree branches out

TABLE 2.4: Data generated at each recursion step

u	π_u	Roots	$\deg_u$	Coeff_u
1	-	$\{0, 5\}$	-1	-
2	1	0	0	0
3	2	3	1	0
4	3	-	2	3
5	1	3	0	5
6	5	5	1	3
7	6	-	2	5

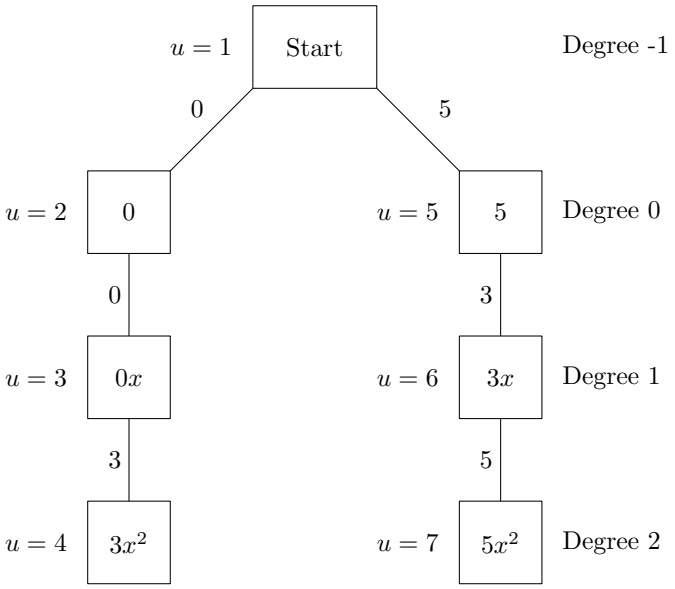


FIGURE 2.8: Tree representation of Roth-Ruckenstein output

whenever more than one root is found in line 6. Lines 8-10 store the current node values and adjust the indices to point to the next node.

Example 2.3 illustrates the Roth-Ruckenstein algorithm.

Example 2.3. *The bivariate polynomial from example 2.2 is used, thus*

$$Q(x, y) = \alpha^2 x^2 + \alpha^6 y + \alpha^6 x^3 + \alpha^3 xy + \alpha^2 x^4 + \alpha^4 x^2 y + y^2 \, .$$

Table 2.4 shows the results generated for each recursion. The two potential messages are thus $0 + 0x + 3x^2$ *and* $5 + 3x + 5x^2$*. An alternative representation is to view the recursion as a tree, as shown in figure 2.8. Each branch of the tree is a canditate message* $\widehat{m}_i$*. In this case, the message on the left corresponds to the transmitted, or causal, codeword.*

Up to this point we have been unconcerned with how the input to the GS algorithm is obtained. The original approach was to only use the hard demodulated symbols as

potential roots and to increase the multiplicity evenly across all roots [41]. We now look at an alternative technique that turns the GS algorithm into a soft-input list decoder, offering further performance improvements.

2.3.3.4 Koetter-Vardy algorithm

The Koetter-Vardy algorithm [42] is a technique for optimally selecting multiplicities of roots for the Guruswami-Sudan algorithm. The input to the algorithm is a $||\mathcal{A}|| \times n$ matrix P which contains entries p_{ij}. The value of each p_{ij} is the probability that the jth element of the codeword is equal to the ith symbol in the alphabet. Bayes' theorem [47] can be used to determine the entries in the probability matrix. Given a transmitted codeword $\mathbf{x}$ with entries from $\mathcal{A}$ and a complex valued received vector $\mathbf{y}$,

$$P(x_j = a_i|y_j) = \frac{P(y_j|x_j = a_i)P(x_j = a_i)}{P(y_j)} \tag{2.51}$$

$$\therefore \quad p_{ij} = \frac{P(y_j|x_j = a_i)}{P(y_j)} \ . \tag{2.52}$$

Equation 2.52 holds provided x_j is uniformly distributed across $\mathcal{A}$. The denominator essentially normalises the probabilities so that

$$\sum_{i=1}^{||\mathcal{A}||} \frac{P(y_j|x_j = a_i)}{P(y_j)} = 1 \ . \tag{2.53}$$

The numerator of equation 2.52 is the likelihood of the channel introducing noise to cause y_j to be a Euclidean distance of n_j from x_j. In an AWGN channel this will be derived from the Gaussian distribution.

The output of the algorithm is the multiplicity matrix M, which is of the same size as P. The entries m_{ij} are the multiplicity of the root (α_j, q_i), where q_i is the ith symbol in the alphabet.

The multiplicity matrix is initially zero, but the entry corresponding to the largest p_{ij} is iteratively increased, while simultaneously scaling down p_{ij}. If this iterative process is repeated indefinitely, the final M matrix will be proportional to the initial P matrix.

The stopping condition is based on the relationship between the cost C of the multiplicity matrix and the desired length of the output list of potential messages, L. A multiplicity matrix with a cost exceeding $C_{\min}$ will result in an output list length up to L.

The cost of the matrix is defined as

$$C = \frac{1}{2} \sum_{i,j} m_{ij}(m_{ij} + 1) \ . \tag{2.54}$$

An intuitive explanation to the cost is that it is initially zero, but incrementing m_{ij} causes C to increase by the new value of m_{ij}.

The minimum cost $C_{\min}$ for a chosen list length L is given as the smallest cost which satisfies the following conditions [42]:

$$L \leq \left\lfloor \frac{\Delta_{1,k-1}(C)}{k-1} \right\rfloor \ , \tag{2.55}$$

$$\text{where} \quad \Delta_{1,k-1}(C) \triangleq \min\{\delta \in \mathbb{Z} \ : \ N_{1,k-1} > C\} \tag{2.56}$$

$$\text{and} \quad N_{1,k-1} \triangleq \left\lceil \frac{\delta+1}{k-1} \right\rceil \left(\delta - \frac{k-1}{2} \left\lfloor \frac{\delta}{k-1} \right\rfloor + 1 \right) \ . \tag{2.57}$$

Algorithm 4: Koetter-Vardy algorithm (from [42])

Data: Probability matrix P

Result: Multiplicity matrix M

initialise $M = \mathbf{0}$, $C = 0$;

while $C < C_{\min}$ **do**

$(i, j) = \underset{i,j}{\text{argmax}}(p_{ij})$;

$p_{ij} = \frac{p_{ij}}{m_{ij}+2}$;

$m_{ij} = m_{ij} + 1$;

$C = C + m_{ij}$;

end

It is demonstrated in [42] that this extension to the GS algorithm introduces a significant gain over the Guruswami-Sudan bound for all list lengths greater than two. This can be ascribed to the fact that low reliability symbols will have few or zero factors, which causes the decoder to behave similarly to an errors and erasures decoder. The KV extension to the GS algorithm increases the number of errors that can be corrected, but there is

no fixed bound for the error correcting capability. Justesen [48] derived expressions for the error correcting capability under several common conditions. He showed that the greatest increase over the hard decision bound was found in three cases: low code rate, subsets of symbols having a large difference in reliability, and when there are very few alternative transmitted symbols.

In summary, the MIMO channel and transmission schemes were investigated along with Reed-Solomon error correction coding and soft decision decoding techniques. In the following chapter, these components will be combined to form a simulated system which can be used to address the research problem.

Chapter 3

Research Methodology

The research methodology was developed so as to satisfy the goals of the research problem, which is to

> Investigate the feasibility of using low rate channel codes as an alternative to transmit diversity in MIMO systems.

The experimental setup must thus be capable of comparing two types of MIMO systems with the same overall rate. The one type of system will use a high rate channel code in conjunction with a low rate (i.e. high diversity) MIMO scheme, while the other type will use a low rate channel code with a high rate MIMO scheme.

3.1 Experimental setup

The research is performed using simulations run in MATLAB [7]. Feasibility of systems is determined by comparing the symbol error rate of the systems across a range of signal to noise ratios. A system is considered infeasible if it performs more than 1 dB worse than the best performing system.

The mimimum number of symbol errors required for each data point is chosen to be proportional to the number of information symbols in each codeword, k. This produces reasonably consistent graph smoothness across all code rates. Due to the increased complexity of soft decision decoding, Guruswami-Sudan simulations are limited to $15k$ symbol errors while Berlekamp-Massey simulations are limited to $100k$ symbol errors.

The MIMO configuration used has two transmitting and two receiving antennas. Due to space limitations in end user equipment, MIMO schemes with two or at most four transmitting and receiving antennas are most common [12–14]. A Rayleigh fading channel is used as this models a rich scattering environment, as encountered in indoor and heavily built up environments [2, 8].

Three different MIMO schemes are simulated: one system with rate 1 and two systems with rate 2. The rate 1 scheme is the Alamouti scheme [28], which is an orthogonal space time block code (STBC) specifically designed for 2×2 systems. The rate 2 schemes are VBLAST [3] and TBLAST [32], which have identical transmission structures but differ in the decoding algorithm.

The system uses 16-QAM modulation. Reed-Solomon channel coding [5] is used with a symbol size of four bits so that each modulation symbol maps to a single code symbol. To achieve the longest possible codewords given the size of the symbol space, the codeword length is $n = 15$. The message size is $k = 5$ for the low rate code, while the high rate simulations are performed using $k = 9$ and $k = 10$.

Both hard and soft decision decoding are implemented – the hard decision decoding is implemented using the Berlekamp-Massey algorithm [40, 43]. Soft decision decoding is used since it can decode beyond the conventional error correcting ability of the code and is particularly suited to low rate codes [41]. The Guruswami-Sudan algorithm [41] is used along with the Koetter-Vardy algorithm [42] for soft decision decoding.

The four comparisons listed below are made, with the final one being the primary objective of the research.

1. The optimal RS code rate for each of the MIMO schemes as well as a SISO AWGN channel.
2. VBLAST vs. TBLAST at various coding rates.
3. Hard decision decoding vs. soft decision decoding for all three MIMO schemes, using both high and low rate codes.
4. High rate MIMO with low rate channel code vs. low rate MIMO with high rate channel code.

All comparisons are plotted as Symbol Error Rate vs. $\frac{E_s}{N_0}$, i.e. the fraction of the message symbols which are incorrectly decoded at the receiver against the ratio of the energy per transmitted information symbol and the noise spectral density. Using $\frac{E_s}{N_0}$ as the controlled variable allows a fair comparison to be made between codes having different rates.

3.2 System description

The simulated system consists of an input data stream, Reed-Solomon encoding, 16-QAM modulation, interleaving, MIMO encoding, block fading Rayleigh channel with AWGN, followed by MIMO decoding, deinterleaving, demodulation and Reed-Solomon decoding.

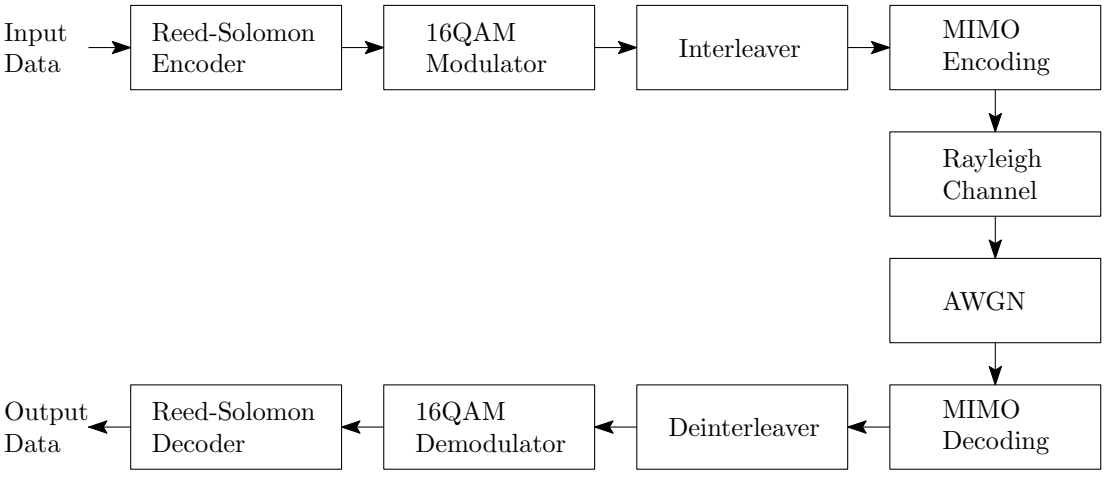


FIGURE 3.1: System Overview

3.2.1 Reed-Solomon

To align Reed-Solomon symbols to modulation symbols, RS symbols are chosen to have a size of 4 bits. This limitation on the number of elements in the RS symbol alphabet restricts the RS codewords to a maximum length of $n = 15$. Longer codes generally perform better than short codes, so codewords are generated at the longest possible length, i.e. 15. The message length k is adjusted depending on the simulation: hard and soft decision decoding is compared using both $(15, 9)$ and $(15, 5)$ codes. In order to compare high diversity (low rate), high RS rate systems to low diversity (high rate), low

RS rate systems: $(15, 10)$ codes over a rate 1 MIMO scheme are compared to $(15, 5)$ RS codes over a rate 2 MIMO scheme.

Reed-Solomon codes with odd values of $n-k$, such as the $(15, 10)$ code, are not typically used as error correcting codes. This is because increasing k by one will offer the same conventional error correcting capability but higher rate. However, since soft decision decoding is performed in this case, the conventional error correcting capability does not impose a hard limit on the error correcting capability and there is no penalty for using odd $n - k$.

Systematic Reed-Solomon encoding is used, allowing a noisy estimate of the message to be extracted even when a decoding failure occurs. The Reed-Solomon subsystem can be set up to either perform hard or soft decision (HD or SD) decoding. The Berlekamp-Massey algorithm is used for HD decoding. For SD decoding, the Guruswami-Sudan (GS) algorithm [41] is used in conjunction with the Koetter-Vardy algorithm [42] for selecting multiplicities of roots. The maximum output list length parameter for the KV algorithm is set to 4 – this outperforms the bound on the GS algorithm while maintaining moderate complexity.

SD decoding outputs a list of messages – only the most likely message is considered for error rate analysis. The most likely message is selected as follows: all messages on the list are re-encoded and modulated to give the expected transmitted vector. The Euclidean distance between the transmitted vector and the received vector is then measured. The message which results in the minimum total distance is selected as the most likely message. If the decoder fails to produce any candidate messages, the systematic portion of the received vector is output as the most likely message.

All error analysis is performed using symbol error rate, i.e. the fraction of symbols from the transmitted message which are decoded erroneously. When the decoders fail to decode the received vector, the systematic portion of the received vector is output as the most likely message.

Using $k = 10$ is preferable for the high rate simulations, as this results in exactly double the code rate of a $k = 5$ system. For hard decision decoding, however, a $(15, 10)$ code has the same error correcting capability as a $(15, 11)$ code, but with a lower rate.

Soft decision decoding simulations thus use $(15, 10)$ codes while hard decision decoding simulations use $(15, 9)$ codes.

3.2.2 MIMO schemes

The MIMO antenna arrangement for this research is a 2×2 system, i.e. two transmitting and two receiving antennas. Due to space limitations in devices, this is one of the more common MIMO configurations [12–14]. Three MIMO encoding schemes are considered: the VBLAST scheme [3], the TBLAST scheme [32] and the Alamouti scheme [28].

The VBLAST scheme transmits an independent symbol over each antenna during each time slot. For a 2×2 system, VBLAST thus transmits two symbols per time slot, which means it is a rate 2 scheme. Decoding is performed by decoding the transmitted symbol with the highest contribution to the received vector first, based on the trained channel matrix. The other symbol is nulled for the first step, i.e. assumed to be equal to zero. The first symbol is quantised to the nearest value from the modulation constellation, following which its contribution is cancelled from the received vector. The second symbol is then decoded. The VBLAST scheme has been discussed in more detail in section 2.2.1.

Quantising the decoded symbols (soft values) to constellation points (hard output) is an inherent part of the VBLAST algorithm. In order to use a soft input Reed-Solomon decoding algorithm, the VBLAST algorithm was adapted to provide a soft output. The final symbol to be decoded is the only symbol for which the decision statistic is generated with full knowledge of the rest of the symbols. The soft value for this symbol is thus simply the decision statistic before the quantisation step. For the symbols that were decoded with only partial knowledge of the co-antenna interference, the known symbols must be substituted back into the original received vector and $\mathbf{G}$ matrix to recover a true soft output (algorithm 1 lines 9 and 7).

Turbo-BLAST, or TBLAST, was developed by Sellathurai and Haykin to minimise the effects of co-antenna interference (CAI). The transmission works identically to VBLAST, so it is also a rate 2 scheme for a 2×2 system. Decoding is performed by iteratively estimating the values for all symbols in the received vector, based on the previously estimated values of the other symbols. As the number of iterations becomes large, the symbol estimates approach the actual values. Since each symbol's estimate is generated

TABLE 3.1: Alamouti STBC structure

	t_0	t_1
TX1	x_0	$-x_1^*$
TX2	x_1	x_0^*

using knowledge of other symbols' estimates, the impact of CAI is minimised. See section 2.2.2 for a more thorough introduction to TBLAST.

For TBLAST to produce a hard output, the expected values are quantised to the constellation points. The soft output values, on the other hand, are simply the expected values for each symbol (equation 2.14).

Neither of the BLAST schemes offer any transmit diversity, only contributing receive diversity in the form of two receive antennas. The diversity order for both BLAST schemes is thus 2.

The Alamouti scheme is an orthogonal space-time block code (STBC) which is only applicable to 2×2 MIMO systems. It utilises two time slots for every two symbols that are transmitted, so it is a rate 1 scheme. Table 3.1 shows the structure of the Alamouti STBC. The decoder uses maximal ratio combining (MRC) to recover the transmitted symbols. MRC works by multiplying the received vector by the complex conjugate of the channel matrix to give the decision statistic [10].

The Alamouti scheme offers a transmit diversity of 2 and a receive diversity of 2, yielding an overall diversity order of 4.

3.2.3 Modulation and channel model

The channel is modelled as a block fading Raleigh channel. The 2×2 channel transfer matrix $\mathbf{H}$ is comprised of independent and identically distributed Rayleigh random variables h_{ij}. These entries have normally distributed real and imaginary components that have zero mean and $\frac{1}{\sqrt{2}}$ variance [11]. The channel matrix is also normalised so that $\mathrm{E}\left[|h_{ij}|^2\right] = 1$ [11]. Following every fading block, a new channel matrix is generated which is independent of all previous channel matrices.

The $\mathbf{H}$ matrix in a real system would be estimated at the receiver by means of a training sequence. For the purposes of these simulations, however, perfect channel knowledge is

assumed at the receiver. The transmitter, however, does not have any channel state information. Both the transmitting antennas thus operate at the same power level.

In order to mitigate the effects of a highly correlated channel matrix, a block interleaver is used. The size of the interleaver is chosen to be sufficiently large that no two symbols in a codeword occur within the same fading block.

The modulation scheme used is rectangular 16-QAM. Since one modulation symbol corresponds to one RS symbol, the ordering of symbols in the constellation (e.g. Gray coding) is of no consequence.

Chapter 4

Results

The primary objective of this research is to compare MIMO systems with equal overall rate but differing MIMO rates and error correcting code rates. The data generated in order to perform this comparison can also be used to draw several other conclusions.

This chapter is structured as follows: to justify the selection of code rates, section 4.1 evaluates a range of rates using each of the MIMO schemes. The preferred high rate MIMO scheme is then selected by comparing VBLAST and TBLAST in section 4.2. Section 4.3 analyses the impact of using soft decision decoding with various code rates over all three MIMO channels. Finally, systems with equal overall rates are compared in section 4.4, which addresses the research problem.

4.1 Optimal code rates

When performing comparisons between different rate codes, it is important to keep the total energy transmitted per message symbol constant. Suppose the reference value of the energy per symbol E_s is based on an uncoded data stream. If an (n, k) code were used and each of the n symbols were transmitted using E_s energy, the total energy used to transmit the stream would be $\frac{n}{k}$ times higher than the reference data stream. It would thus achieve lower error rates than the reference stream not solely due to the error correcting code, but also due to the higher signal to noise ratio. When using error correcting codes it is thus necessary to spread the energy from the reference message

across all the codeword symbols to maintain a fair comparison. Each codeword symbol is therefore transmitted using $\frac{k}{n}E_s$ energy.

It is well known that low rate codes are capable of correcting more errors than high rate codes due to offering a larger minimum distance. This, however, comes at the expense of reduced energy per codeword symbol. Reduced energy per codeword symbol results in more errors that need to be corrected, which counteracts the error correcting improvement.

The fact that error correction codes offer a gain over uncoded systems indicates that the error correcting improvement is greater than the energy decrease. This is not true for all code rates though. Consider a trivial $(15, 1)$ code: the same symbol is transmitted 15 times with an energy of $\frac{1}{15}E_s$. Theoretical models using MATLAB's `bertool` [7] show that such a code actually performs more than 3 dB worse than an uncoded system in an AWGN environment. There is therefore a point at which decreasing the code rate will not provide any further improvements in error rate.

The error rate curves for RS codes of length 15 with HD decoding in a SISO AWGN channel are shown in figure 4.1. The $(15, 9)$ RS code offers the best performance, but the $(15, 11)$ and $(15, 7)$ codes offer comparable performance at an SER of 10^{-4}. The $(15, 5)$ code performs 0.9 dB worse than the $(15, 9)$ code. This state of affairs is not the case for all channel models, though, as demonstrated below.

The SISO Rayleigh fading channel as implemented in this research causes some fading blocks to experience a decreased $\frac{E_s}{N_0}$, since the scalar H attenuates the transmitted signal power. Due to the perfect channel state information available at the receiver, however, the phase of H has no effect. Due to the attenuated signal, symbols in poor fading blocks are therefore more likely to be decoded incorrectly. This is expected to result in lower rate codes exhibiting better performance relative to high rate codes than in the SISO AWGN case. To verify this, figure 4.2 shows the error rate curves for a SISO block fading Rayleigh channel. The performance of all code rates is degraded due to the Rayleigh fading, but the $(15, 5)$ RS code exhibits the best performance, followed closely by the $(15, 7)$ and $(15, 3)$ codes. The $(15, 9)$ RS code performs 1.9 dB worse than the $(15, 5)$ code.

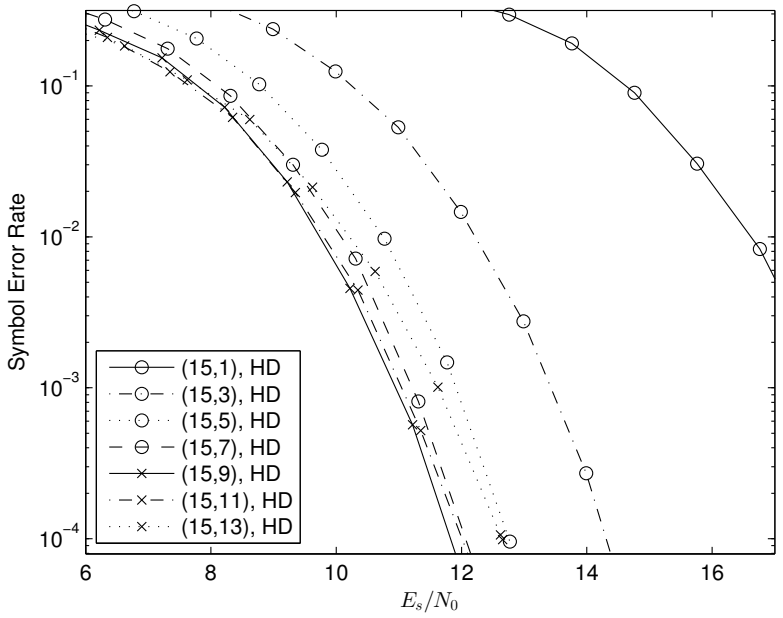


FIGURE 4.1: Comparison of code rates in an AWGN environment

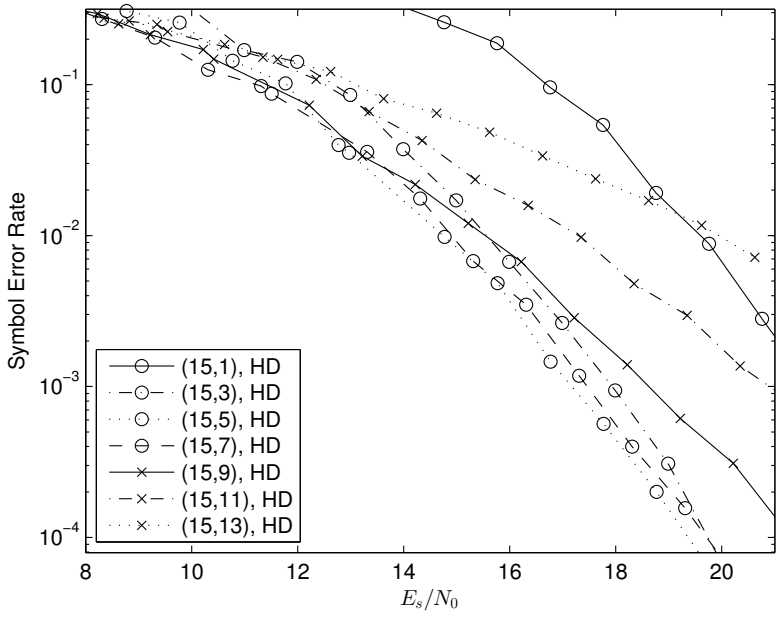


FIGURE 4.2: Comparison of code rates in a SISO Rayleigh environment

Figures 4.3, 4.4 and 4.5 show the results of comparing various rate RS codes using the Alamouti STBC, VBLAST and TBLAST respectively.

Using the Alamouti scheme, it is evident from figure 4.3 that the $(15, 7)$ RS code achieves a symbol error rate of 10^{-4} at the lowest E_s/N_0. It narrowly outperforms the $(15, 9)$ code by 0.05 dB. The margin between the $(15, 9)$ and $(15, 5)$ RS codes is 0.4 dB. Comparing

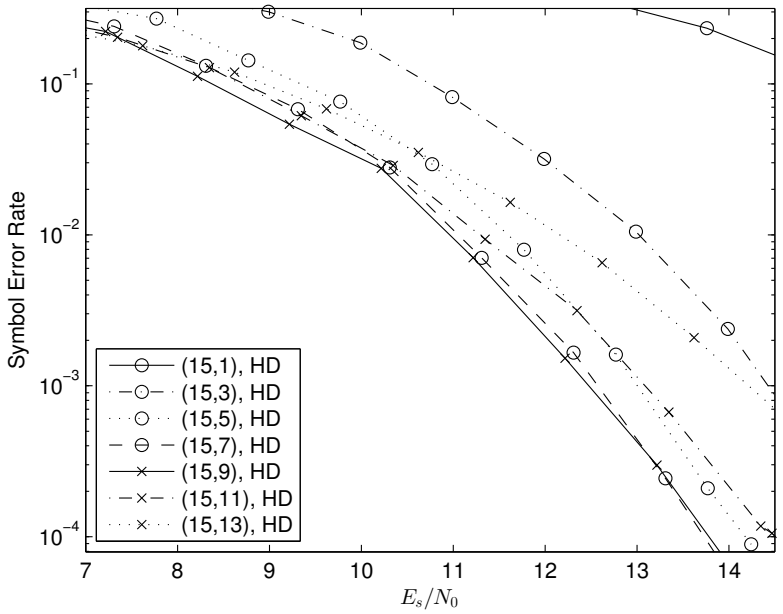


FIGURE 4.3: Comparison of code rates in an Alamouti MIMO environment

these results to the equivalent SISO Rayleigh fading results in figure 4.2, the Alamouti encoding scheme offers approximately a 6 dB improvement in performance of the best codes rates. The best codes rates for a channel experiencing only AWGN, however, still outperform the Alamouti scheme in a Rayleigh fading channel by almost 2 dB. This indicates that the Alamouti scheme counteracts most, but not all, of the negative impact of Rayleigh fading.

The optimal code rate is not the same for all MIMO schemes, though. When utilising the VBLAST scheme, as depicted in figure 4.4, the $(15, 5)$ code offers the best performance, achieving an SER of 10^{-4} at an E_s/N_0 of 19.7 dB, closely followed by the $(15, 7)$ code. The $(15, 9)$ code performs 1.4 dB worse than the $(15, 5)$ code. These results resemble the results from the SISO Rayleigh fading channel, where the best performing code rate achieved an SER of 10^{-4} at an E_s/N_0 of 19.4 dB. This confirms that the lack of diversity in the VBLAST scheme causes it to be hampered by Rayleigh fading in a similar fashion to a SISO system.

The improved performance of low rate RS codes compared to high rate RS codes is explained by considering the propagation of symbol errors within the VBLAST structure. When the first symbol in the VBLAST decoding process produces an error, the incorrect

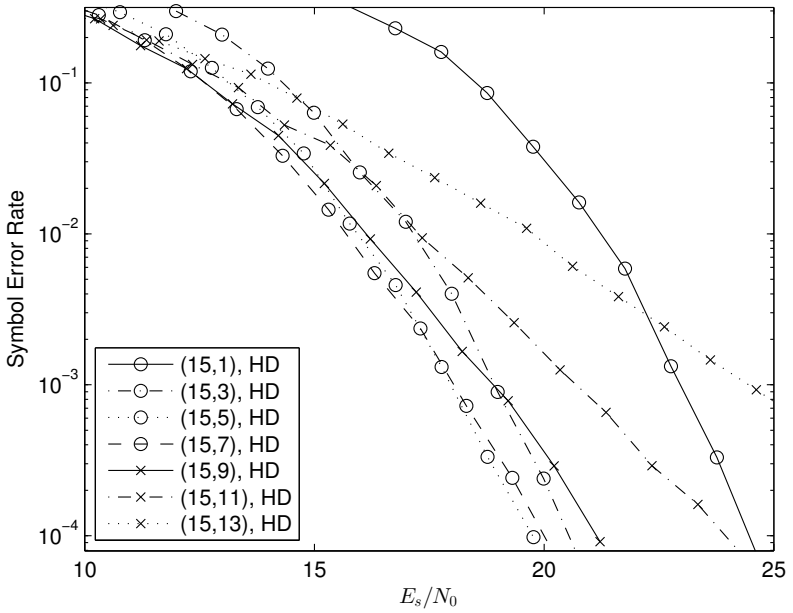


FIGURE 4.4: Comparison of code rates in a VBLAST MIMO environment

value is used in the cancelling process. The second symbol is thus decoded using erroneous information, dramatically increasing the error probability of the second symbol as well. This interdependence of symbols results in additional errors, requiring greater error correcting capability from the channel code. Although the interleaver minimises the impact of error propagation on single codewords, the effect remains noticeable due to cross-propagation of errors from different codewords.

The TBLAST scheme, as shown in figure 4.5, exhibits very similar properties to VBLAST; with the optimal code rate being lower than that for the SISO AWGN channel. Once again the $(15, 5)$ code performs best, followed by the $(15, 7)$ and $(15, 3)$ RS codes respectively. The $(15, 9)$ code performs 1.7 dB worse than the best performing code.

Errors in the TBLAST scheme do not propagate sequentially from one incorrectly decoded symbol to another, but occur when the expected values of both symbols iteratively tend away from the correct values. This can be caused by either poor signal-to-noise ratio or a spatially correlated channel matrix. Although the error propagation mechanism is different between the two BLAST schemes, they exhibit very similar behaviour.

Based on the results in this section, the best error rates are achieved using $(15, 5)$ RS codes with the BLAST based schemes and $(15, 7)$ or $(15, 9)$ codes with the Alamouti scheme. To achieve the objectives of this research, two code rates must be selected

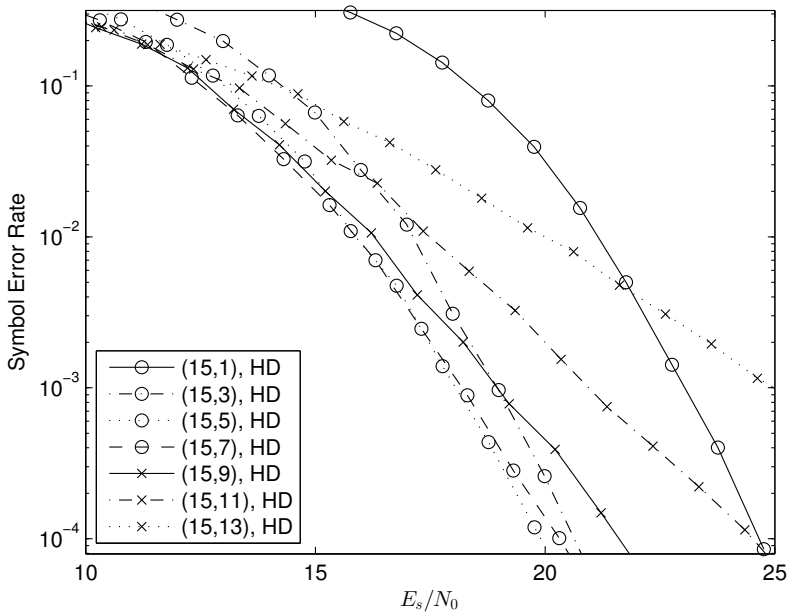


FIGURE 4.5: Comparison of code rates in a TBLAST MIMO environment

such that the RS code rate for the VBLAST scheme is half of the RS code rate for the Alamouti scheme. Normally, odd values of $n-k$ are not used in Reed-Solomon codes, as the conventional error correcting capability is $\left\lfloor \frac{n-k}{2} \right\rfloor$. In this research, however, the Koetter-Vardy soft decision decoding algorithm is used, which is less dependent on using even values of $n-k$. A natural selection for two codes where the ratio of rates is 2 is thus the $(15, 5)$ and $(15, 9)$ codes, with $(15, 10)$ codes being used with soft decision decoding.

4.2 VBLAST vs TBLAST

The two BLAST based schemes use an identical transmission structure, i.e. transmitting independent streams of information over each antenna. TBLAST offers better performance on systems with many transmit and receive antennas, as shown by Sellathurai and Haykin [32]. This is due to improved handling of co-antenna interference (CAI). On systems with few antennas, such as the 2×2 system used in this research, CAI does not constitute as large a fraction of the total received power. VBLAST is therefore less likely to erroneously decode the first symbol for systems with few antennas than systems with many antennas.

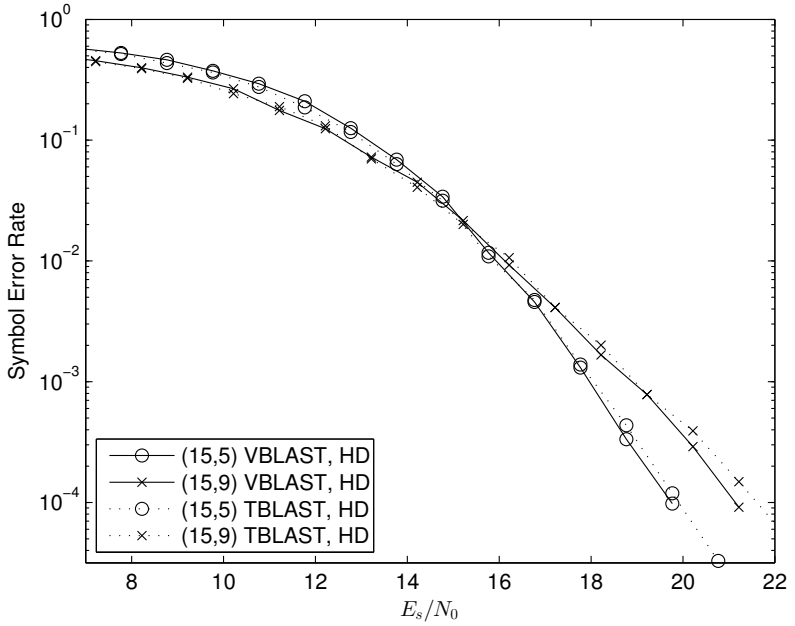


FIGURE 4.6: Comparison of VBLAST and TBLAST using the Berlekamp-Massey decoding algorithm

Figures 4.6 and 4.7 show the performance of the two BLAST based schemes using hard and soft decision decoding respectively. It is evident that VBLAST and TBLAST offer similar performance, but VBLAST offers marginally better performance at an error rate of 10^{-4} for all four rate/decoding combinations. With hard decision decoding VBLAST outperforms TBLAST by 0.2 and 0.5 dB for the $(15, 5)$ and $(15, 9)$ codes respectively. With SD decoding, VBLAST outperforms TBLAST by 0.1 and 0.4 dB for the low and high rate codes respectively.

Although TBLAST may offer a significant gain for large antenna systems, this performance increase is not evident when there are only two transmitting and receiving antennas. This is explained by considering the energy contribution of the desired symbol and the co-antenna interference. With two transmitting antennas, the expected CAI energy is equal to the expected symbol energy, resulting in a signal-to-CAI ratio (SCR) of 0 dB. With 16 transmitting antennas, the expected CAI energy is 15 times greater than the expected symbol energy, which is an SCR of -11.8 dB. It is clear that handling of CAI thus becomes significantly more important when a large number of antennas are present.

The technique of ordering symbol decoding by post-detection SNR as used in VBLAST

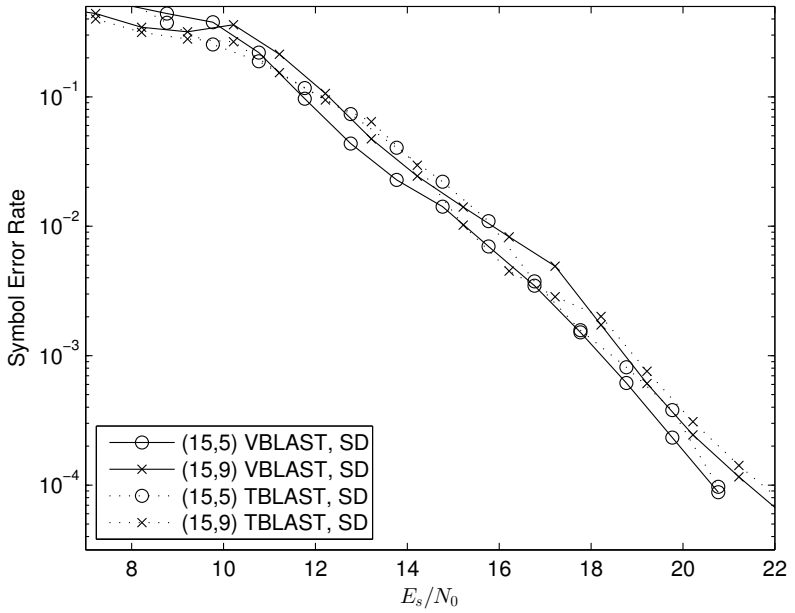


FIGURE 4.7: Comparison of VBLAST and TBLAST using a 2×2 MIMO system and the Koetter-Vardy decoding algorithm

thus provides slightly more of a benefit than iteratively estimating co-antenna interference.

4.3 Soft decision decoding gain

Soft decision (SD) Reed-Solomon decoding can potentially offer an improvement in error rate performance at the expense of significantly increased complexity. Analysing the complexity-performance tradeoff is not the objective of this research, but the performance increase is quantified in this section.

The asymptotic error correcting capability of the Guruswami-Sudan algorithm sans Koetter-Vardy is $n - 1 - \left\lfloor \sqrt{(k-1)n} \right\rfloor$, compared to a hard decision bound of $\lfloor \frac{n-k}{2} \rfloor$. The expected benefit of using soft decision decoding thus increases as the code rate decreases. The Koetter-Vardy algorithm offers performance exceeding the bound of the GS algorithm. The exact error correcting capability can however not be easily quantified, since certain symbol reliability patterns allow more errors to be corrected than others.

The soft decision gain obtained using the KV algorithm is investigated for all three MIMO schemes using $(15, 5)$, $(15, 9)$ and $(15, 10)$ Reed-Solomon codes. Since a $(15, 10)$

code has an error correcting capability of $t = 2$ while a $(15, 9)$ code has $t = 3$, the lower hard decision performance of the former code should result in a larger soft decision gain, as the SD decoder is not as significantly affected by the odd number of parity symbols as the HD decoder. Additionally, it is expected that the $(15, 5)$ code will exhibit a larger SD gain than the higher rate codes due to the higher theoretical error correcting capability.

Figure 4.8 shows error rate performance for the three code rates over an Alamouti channel with hard and soft decoding. This demonstrates the effect of using soft decision decoding on RS codes when there are an odd number of parity symbols. At a symbol error rate of 10^{-4}, the $(15, 9)$ code exhibits a soft decision gain of 0.1 dB, compared to 0.9 dB for the $(15, 10)$ code – a difference of 0.8 dB. It can thus be concluded that the soft decision decoder does not suffer as significant a penalty from an odd number of parity symbols as a hard decision decoder.

When analysing the effect of code rate on soft decision gain, it is thus not practical to include codes with an odd $(n - k)$. This analysis is therefore performed using only the $(15, 5)$ and $(15, 9)$ RS codes. Figures 4.8, 4.9 and 4.10 show the performance of the two selected codes rates in conjunction with the Alamouti, VBLAST and TBLAST schemes respectively. The soft decision gain for all combinations of the two code rates and three MIMO schemes is summarised in table 4.1.

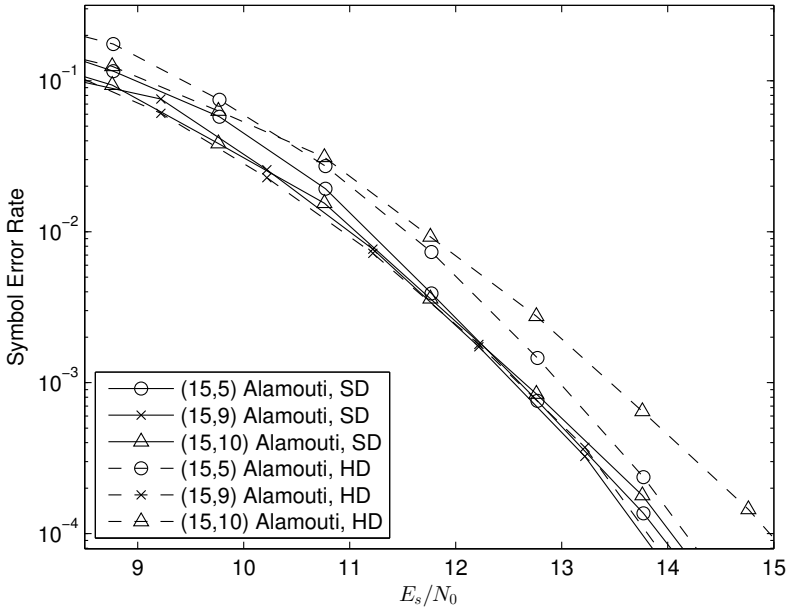


FIGURE 4.8: Comparison of soft and hard decision RS decoding with the Alamouti scheme

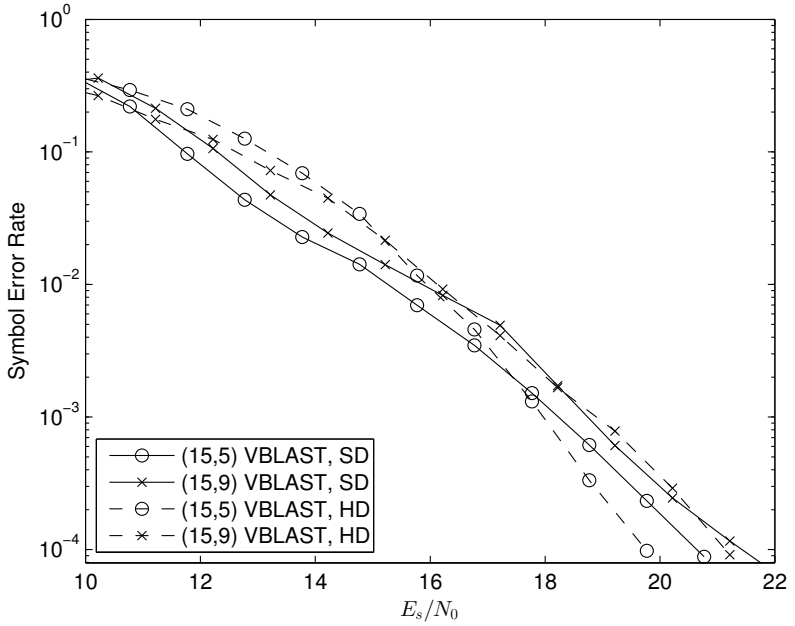


FIGURE 4.9: Comparison of soft and hard decision RS decoding with the VBLAST scheme

TABLE 4.1: Summary of soft decision gains at SER $= 10^{-4}$

	$(15, 5)$	$(15, 9)$	Difference
Alamouti	0.2 dB	0.1 dB	0.1 dB
VBLAST	-1.9 dB	-0.3 dB	-1.6 dB
TBLAST	-1.8 dB	-0.1 dB	-1.7 dB

The results in table 4.1 are somewhat unexpected. The soft decision RS decoder offers very little gain when combined with the Alamouti MIMO scheme, and actually performs significantly worse when combined with the BLAST based schemes. Additionally, while the low rate RS code exhibits a small soft decision decoding gain over the high rate code using the Alamouti scheme, no such gain is evident with the BLAST based schemes. Soft decision RS decoding in fact performs at least 1.6 dB worse at low rate codes than high rate codes when using the BLAST based schemes.

These results suggest that the MIMO schemes – in particular VBLAST and TBLAST – do not generate good quality reliability information. This increases the probability that the SD decoder will select multiple incorrect candidates for each symbol. There are subsequently many non-causal codewords in the list of candidate codewords that the decoder generates, increasing the likelihood of the causal codeword not being selected or potentially even not in the list.

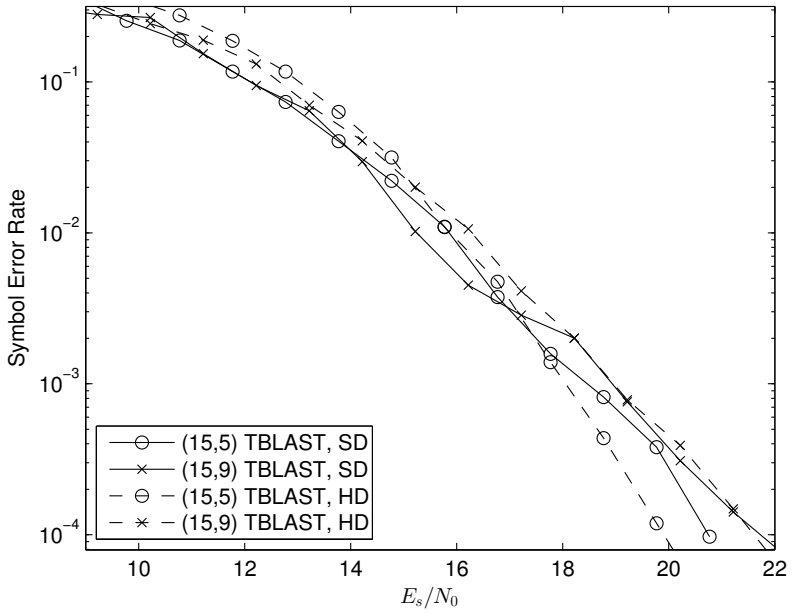


FIGURE 4.10: Comparison of soft and hard decision RS decoding with the TBLAST scheme

Some results that were generated during the course of the research indicate that this result may be dependent on the fading channel model used. Using an incorrect implementation of the Rayleigh fading model, soft decision decoding gains around 1 dB were observed, with the low rate RS codes offering around 0.5 dB more of an SD gain than the high rate codes.

The poor performance of the BLAST based systems is explained by considering the effect of error propagation. Symbol errors in both VBLAST and TBLAST cause the simultaneously transmitted symbol to have reduced reliability. This negatively impacts performance since there are fewer reliable symbols that the decoder can select.

Based on the poor performance of soft decision decoding in these results, there is no justification for using soft decision decoding in the remainder of the research.

4.4 Transmit diversity vs code rate

The primary objective of this research is to investigate the feasibility of using low rate codes as an alternative to diversity. VBLAST is used as the rate 2 MIMO scheme, as it was shown in section 4.2 to offer better performance than TBLAST. VBLAST is

paired with a $(15, 5)$ RS code and is compared to the Alamouti STBC with $(15, 10)$ RS coding, keeping the overall rate of the two systems constant. Since soft decision decoding has been ruled out as a viable option in the previous section and the $(15, 10)$ code doesn't perform well with hard decision decoding, the performance of the $(15, 9)$ RS code using the Alamouti scheme is shown as well. These code rates were also shown in section 4.1 to be optimal or close to optimal for each MIMO scheme. Hard decision (Berlekamp-Massey) RS decoding is used with all three systems: the results are shown in figure 4.11.

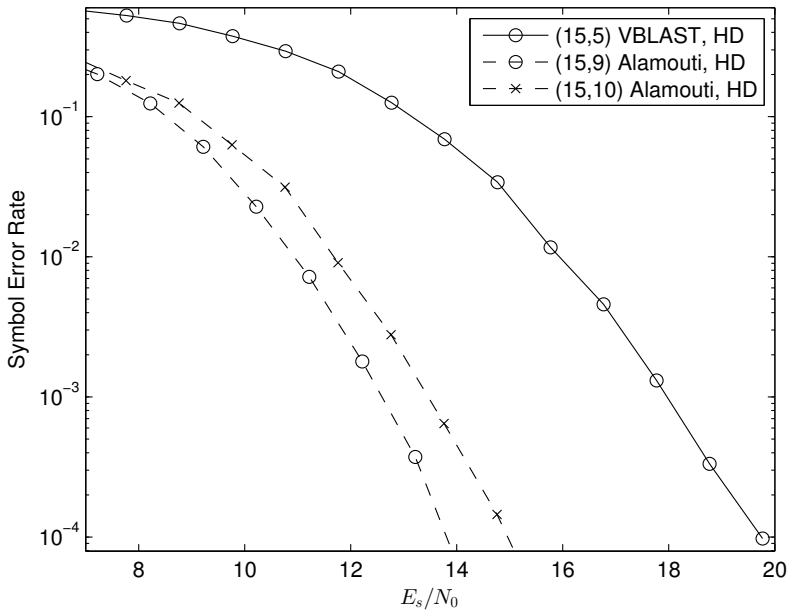


FIGURE 4.11: Comparison of MIMO systems with equal overall rate

As expected, the $(15, 10)$ RS code is hampered by having a lower error correcting ability, performing about 1.1 dB worse than the $(15, 9)$ RS code. The $(15, 9)$ high diversity system outperforms the low diversity system by 5.9 dB at a symbol error rate of 10^{-4}. This is a very large gain – the high diversity system can achieve the same error rates as the low diversity system while using about four times less power. **Low rate error correcting codes are thus not a feasible alternative to transmit diversity in the MIMO systems which were evaluated.**

It can be concluded from this result that increasing transmit diversity is significantly more effective than decreasing code rate for the system simulated. Although this conclusion can only be drawn under the conditions of this simulation, the magnitude of the

margin suggests that similar results are likely to be achieved using different channel models and MIMO schemes. The mechanism by which the high rate system achieves such good performance is that it reduces the number of symbol errors in the received vector before it is passed to the Reed-Solomon decoder. The number of pre-decoding symbol errors eliminated by high diversity exceeds the increase in error correcting capability of the low rate code by a significant margin.

Chapter 5

Conclusion

The main conclusions that were drawn during this research are summarised in this chapter, along with recommendations for future work. The results consisted of four findings:

1. Optimal code rate for various MIMO schemes
2. Preferred high rate MIMO scheme
3. Impact of soft decision decoding
4. Code rate vs. transmit diversity

These findings are summarised in sections 5.1 to 5.4. Finally, recommendations for future work are discussed in section 5.5.

5.1 Optimal code rates

The symbol error rate performance of $(15, k)$ Reed-Solomon codes was measured on SISO AWGN, SISO Rayleigh, MIMO Alamouti, MIMO VBLAST and MIMO TBLAST channels. All odd values of k from 1 to 13 were used. The optimal code rate is the point at which it becomes more effective to increase the transmit power than to further lower the code rate.

While the $(15, 9)$ RS code peformed best over the SISO AWGN channel, the addition of Rayleigh fading favours lower rate codes, with the $(15, 5)$ RS code performing best, albeit almost 8 dB worse than in a channel without Rayleigh fading. The Alamouti channel with Rayleigh fading shows similar characteristics to a SISO AWGN channel: the $(15, 7)$ and $(15, 9)$ RS codes offer the best performance, which is around 2 dB worse than the best SISO AWGN performance. This indicates that the Alamouti STBC succesfully mitigates most of the effects of multipath fading, recovering both symbols in a block even when there is significant spatial correlation.

The various codes behaved somewhat differently when using VBLAST and TBLAST – in both cases the $(15, 5)$ code (rate $\frac{1}{3}$) offered the best performance. The results resemble those using a SISO Rayleigh channel, both in optimal code rate and performance, which shows how the lack of diversity makes the BLAST based schemes susceptible to the adverse effects of Rayleigh fading. The error propagation which occurs in VBLAST and TBLAST also requires greater error correcting capability than orthogonal schemes such as the Alamouti scheme.

It can be concluded that the optimal code rate for any given system is somewhat dependent on the properties of the MIMO scheme. Systems with diversity perform best when combined with high rate codes, while low rate codes are necessary for systems that have no diversity and that exhibit error propagation.

5.2 VBLAST vs TBLAST

The two BLAST schemes were shown to offer very similar performance. Although TBLAST may perform better in systems with many antennas, VBLAST was marginally better with the 2×2 antenna system considered in this research. This suggests that when considering a MIMO systems with few antennas, as used in this research, the technique of ordering symbols by post-detection SNR is slightly more effective than trying to iteratively eliminate CAI.

5.3 Soft decision decoding gain

The least expected result from this research is that soft decision decoding using the Guruswami-Sudan algorithm with the Koetter-Vardy (GS-KV) algorithm is not guaranteed to provide a gain over using hard decision decoding. The SD gain using the Alamouti scheme was less than 0.2 dB, while the BLAST based schemes performed worse with the GS-KV algorithm than with hard decision decoding. Considering the decoding gain reported by [42] and other results generated with invalid channel models, it can be concluded that the amount of gain provided by the GS-KV algorithm is dependent on the channel model used.

The poor performance of VBLAST and TBLAST in conjunction with soft decision decoding is likely due to the way that errors propagate between simultaneously transmitted symbols. The error propagation affects the quality of the reliability information that is passed to the SD decoder, resulting in the poor SD decoding performance.

It was also shown that the soft decision gain when using the $(15, 10)$ code exceeded the gain when using a $(15, 9)$ code. This indicates that the GS-KV algorithm is therefore not as severely affected when using an RS code with an odd value of $(n - k)$ as a hard decision decoder.

5.4 Code rate vs transmit diversity

The research problem was to investigate the feasibility of using low rate channel codes as an alternative to transmit diversity in MIMO systems. This was done by comparing the Alamouti STBC in conjunction with a $(15, 10)$ Reed-Solomon code to the VBLAST scheme with a $(15, 5)$ RS code. The overall rate for the two systems is therefore equal. The first system (with high transmit diversity) outperformed the second scheme (with low code rate) by 4.8 dB. This is a very large margin and indicates that low rate codes are not a feasible alternative to transmit diversity under the conditions that were simulated. Additionally, the $(15, 10)$ code is hampered by only having an error correcting capability of 2; if a $(15, 9)$ code is used the margin between the high diversity and low diversity scheme increases to 5.9 dB. The magnitude of the margin between the two types of

schemes suggests that it is highly improbable that a different conclusion would be drawn even under different simulation conditions.

5.5 Recommendations for future work

Considering the large margin between the low rate / low diversity system and the high rate / high diversity system, recommendations for future work are not intended to be used to narrow the gap between the two types of systems. The recommendations are merely areas of interest for future research.

The error propagation encountered in both BLAST schemes may be better handled by leveraging the burst correction abilities of Reed-Solomon codes. If the size of RS symbols is selected to be n_T times larger than the modulation symbols, every time slot in the BLAST based scheme will correspond to a single RS symbol. For example, if 16-QAM (four bits per symbol) is used with a 2×2 MIMO antenna configuration, the RS symbols should be taken from GF(256) (eight bits per symbol). An error would thus propagate between the lower 4 bits and upper 4 bits of an RS symbol, but would never affect other RS symbols. This should reduce the number of errors that the RS code needs to correct, reducing the likelihood of a decoding failure. A similar technique can be investigated for the Alamouti STBC, but it is not expected to have as much of an impact.

A few simplifying assumptions were made regarding the channel model. A block fading Rayleigh channel was used and perfect channel state information was assumed at the receiver. This made it simple to develop an interleaver which prevents a poor channel from affecting more than one symbol in a codeword and also eliminated errors due to incorrect channel estimation. The impact of different channel models on the performance of the MIMO schemes should be investigated.

The results also suggest that the channel model has a significant impact on the GS-KV soft decision decoding algorithm. Soft decision decoding performed worse than hard decision decoding for the BLAST based schemes and only offered a small gain when combined with the Alamouti scheme. This is unexpected, as prior research [42] using other channel models indicates significant soft decision gain. The impact of various channel models on the performance of the GS-KV decoder should be analysed.

While BLAST based systems do have their place in situations where very high spectral density is required, it would generally be recommended to focus on MIMO schemes that incorporate transmit diversity. Increased transmit diversity makes the system much more resistant to poor channel conditions and results in significantly lower error rates.

Bibliography

[1] J.D. Parsons and A.S. Bajwa. Wideband characterisation of fading mobile radio channels. *Communications, Radar and Signal Processing, IEE Proceedings F*, 129 (2):95–, April 1982. ISSN 0143-7070. doi: 10.1049/ip-f-1.1982.0016.

[2] William C. Jakes and Donald C. Cox, editors. *Microwave Mobile Communications*. Wiley-IEEE Press, 1994. ISBN 0780310691.

[3] P.W. Wolniansky, G.J. Foschini, G.D. Golden, and R. Valenzuela. V-BLAST: an architecture for realizing very high data rates over the rich-scattering wireless channel. In *Signals, Systems, and Electronics, 1998. ISSSE 98. 1998 URSI International Symposium on*, pages 295–300, September 1998. doi: 10.1109/ISSSE.1998.738086.

[4] R. C. Singleton. Maximum Distance q-nary codes. *IEEE Transactions on Information Theory*, 10(2):116–118, Apr 1964.

[5] Irving Reed and Gustave Solomon. Polynomial codes over certain finite fields. *Journal of the Society of Industrial and Applied Mathematics*, 8(2):300–304, 06/1960 1960. URL `http://www.jstor.org/pss/2098968`.

[6] N. Ratnakar and R. Koetter. *Information Theory, IEEE Transactions on*, 51(11): 3899–3917, Nov 2005. ISSN 0018-9448.

[7] MATLAB and Communications Toolbox Release 2014a, The MathWorks, Inc., Natick, Massachusetts, United States.

[8] B. Sklar. Rayleigh fading channels in mobile digital communication systems .I. Characterization. *Communications Magazine, IEEE*, 35(7):90–100, Jul 1997. ISSN 0163-6804. doi: 10.1109/35.601747.

[9] Gerard J Foschini. Layered space-time architecture for wireless communication in a fading environment when using multi-element antennas. *Bell Labs Technical Journal*, 1(2):41–59, 1996.

[10] D.G. Brennan. Linear Diversity Combining Techniques. *Proceedings of the IRE*, 47 (6):1075–1102, June 1959. ISSN 0096-8390. doi: 10.1109/JRPROC.1959.287136.

[11] G. J. Foschini and M. J. Gans. On limits of wireless communications in a fading environment when using multiple antennas. *Wireless Personal Communications*, 6: 311–335, 1998.

[12] IEEE Standard for Information technology – Local and metropolitan area networks – Specific requirements – Part 11: Wireless LAN Medium Access Control (MAC) and Physical Layer (PHY) Specifications Amendment 5: Enhancements for Higher Throughput. *IEEE Std 802.11n-2009 (Amendment to IEEE Std 802.11-2007 as amended by IEEE Std 802.11k-2008, IEEE Std 802.11r-2008, IEEE Std 802.11y-2008, and IEEE Std 802.11w-2009)*, pages 1–565, Oct 2009. doi: 10.1109/IEEESTD.2009.5307322.

[13] IEEE Standard for Information technology – Telecommunications and information exchange between systems. Local and metropolitan area networks – Specific requirements – Part 11: Wireless LAN Medium Access Control (MAC) and Physical Layer (PHY) Specifications–Amendment 4: Enhancements for Very High Throughput for Operation in Bands below 6 GHz. *IEEE Std 802.11ac-2013 (Amendment to IEEE Std 802.11-2012, as amended by IEEE Std 802.11ae-2012, IEEE Std 802.11aa-2012, and IEEE Std 802.11ad-2012)*, pages 1–425, Dec 2013. doi: 10.1109/IEEESTD.2013.6687187.

[14] ETSI. 3GPP TS 36.213 Evolved Universal Terrestrial Radio Access (E-UTRA); Physical layer procedures. Technical report, `www.etsi.org`, 2014.

[15] F. Boccardi, B. Clerckx, A. Ghosh, E. Hardouin, G. Jöngren, K. Kusume, E. Onggosanusi, and Yang Tang. Multiple-antenna techniques in LTE-advanced. *Communications Magazine, IEEE*, 50(3):114–121, March 2012. ISSN 0163-6804. doi: 10.1109/MCOM.2012.6163590.

[16] R.W.E. McNicol. The fading of radio waves of medium and high frequencies. *Proceedings of the IEE - Part III: Radio and Communication Engineering*, 96(44): 517–524, November 1949. doi: 10.1049/pi-3.1949.0108.

[17] D. Chizhik, J. Ling, P.W. Wolniansky, R.A. Valenzuela, N. Costa, and K. Huber. Multiple-input-multiple-output measurements and modeling in Manhattan. *Selected Areas in Communications, IEEE Journal on*, 21(3):321–331, Apr 2003. ISSN 0733-8716. doi: 10.1109/JSAC.2003.809457.

[18] H. Nishimoto, Y. Ogawa, T. Nishimura, and T. Ohgane. Measurement-Based Performance Evaluation of MIMO Spatial Multiplexing in a Multipath-Rich Indoor Environment. *Antennas and Propagation, IEEE Transactions on*, 55(12):3677–3689, Dec 2007. ISSN 0018-926X. doi: 10.1109/TAP.2007.910303.

[19] U. Schilcher, C. Bettstetter, and G. Brandner. Temporal Correlation of Interference in Wireless Networks with Rayleigh Block Fading. *Mobile Computing, IEEE Transactions on*, 11(12):2109–2120, Dec 2012. ISSN 1536-1233. doi: 10.1109/TMC.2011.244.

[20] M.S. Raju, R. Annavajjala, and A. Chockalingam. BER analysis of QAM on fading channels with transmit diversity. *Wireless Communications, IEEE Transactions on*, 5(3):481–486, March 2006. ISSN 1536-1276. doi: 10.1109/TWC.2006.1611074.

[21] M. Klessling, J. Speidel, and Yejian Chen. MIMO channel estimation in correlated fading environments. In *Vehicular Technology Conference, 2003. VTC 2003-Fall. 2003 IEEE 58th*, volume 2, pages 1187–1191 Vol.2, Oct 2003. doi: 10.1109/VETECF.2003.1285209.

[22] N. Shariati, Jiaheng Wang, and M. Bengtsson. Robust Training Sequence Design for Correlated MIMO Channel Estimation. *Signal Processing, IEEE Transactions on*, 62(1):107–120, Jan 2014. ISSN 1053-587X. doi: 10.1109/TSP.2013.2284763.

[23] Yen-Chih Chen and Yu-T Su. MIMO channel estimation in correlated fading environments. *Wireless Communications, IEEE Transactions on*, 9(3):1108–1119, March 2010. ISSN 1536-1276. doi: 10.1109/TWC.2010.03.081603.

[24] R.C. de Lamare and R. Sampaio-Neto. Blind adaptive MIMO receivers for space-time block-coded DS-CDMA systems in multipath channels using the constant modulus criterion. *Communications, IEEE Transactions on*, 58(1):21–27, January 2010. ISSN 0090-6778. doi: 10.1109/TCOMM.2010.01.070549.

[25] D. Chase and Lih-Jyh Weng. Multiple-burst correction techniques for slowly fading channels. *Information Theory, IEEE Transactions on*, 22(5):505–513, Sep 1976. ISSN 0018-9448. doi: 10.1109/TIT.1976.1055616.

[26] Seyeong Choi, Young-chai Ko, and E.J. Powers. Optimization of Switched MIMO Systems Over Rayleigh Fading Channels. *Vehicular Technology, IEEE Transactions on*, 56(1):103–114, Jan 2007. ISSN 0018-9545. doi: 10.1109/TVT.2006.883748.

[27] L.C. Godara. Application of antenna arrays to mobile communications. II. Beamforming and direction-of-arrival considerations. *Proceedings of the IEEE*, 85(8): 1195–1245, Aug 1997. ISSN 0018-9219. doi: 10.1109/5.622504.

[28] S. Alamouti. A simple transmit diversity technique for wireless communications. *Selected Areas in Communications, IEEE Journal on*, 16(8):1451–1458, Oct 1998. ISSN 0733-8716. doi: 10.1109/49.730453.

[29] Chong Han, Xiaomin Zhang, and Yu Chen. A novel full density QSTBC scheme with low complexity. In *Image and Signal Processing (CISP), 2013 6th International Congress on*, volume 03, pages 1478–1482, Dec 2013. doi: 10.1109/CISP.2013.6743908.

[30] H. Lee. Robust full-diversity full-rate quasi-orthogonal STBC for four transmit antennas. *Electronics Letters*, 45(20):1044–1045, September 2009. ISSN 0013-5194. doi: 10.1049/el.2009.0481.

[31] G. H. Golub and C. F. Van Loan. *Matrix Computations*. Johns Hopkins University Press, Baltimore, MD, USA, 3rd edition, 1996. ISBN 0-8018-5414-8.

[32] M. Sellathurai and S. Haykin. TURBO-BLAST for high-speed wireless communications. In *Wireless Communications and Networking Confernce, 2000. WCNC. 2000 IEEE*, volume 1, pages 315–320 vol.1, 2000. doi: 10.1109/WCNC.2000.904649.

[33] Vahid Tarokh, Hamid Jafarkhani, and A.R. Calderbank. Space-time block codes from orthogonal designs. *Information Theory, IEEE Transactions on*, 45(5):1456–1467, Jul 1999. ISSN 0018-9448. doi: 10.1109/18.771146.

[34] Hamid Jafarkhani. A quasi-orthogonal space-time block code. *Communications, IEEE Transactions on*, 49(1):1–4, Jan 2001. ISSN 0090-6778. doi: 10.1109/26.898239.

[35] Chau Yuen, Yong Liang Guan, and Tjeng-Thiang Tjhung. Quasi-orthogonal STBC with minimum decoding complexity. *Wireless Communications, IEEE Transactions on*, 4(5):2089–2094, Sept 2005. ISSN 1536-1276. doi: 10.1109/TWC.2005.853890.

[36] Haiquan Wang, Dong Wang, and Xiang-Gen Xia. On Optimal Quasi-Orthogonal Space-Time Block Codes With Minimum Decoding Complexity. *Information Theory, IEEE Transactions on*, 55(3):1104–1130, March 2009. ISSN 0018-9448. doi: 10.1109/TIT.2008.2011521.

[37] Shu Lin and Daniel J. Costello. *Error Control Coding, Second Edition*. Prentice-Hall, Inc., Upper Saddle River, NJ, USA, 2004. ISBN 0130426725.

[38] International Telecommunication Union. G.992.1 : Asymmetric digital subscriber line (ADSL) transceivers. Technical report.

[39] S.B. Wicker and V.K. Bhargava. *Reed-Solomon Codes and Their Applications*. Wiley, 1999. ISBN 9780780353916. URL `http://books.google.co.za/books?id=yws55Rx1orEC`.

[40] MathWorks Documentation Center. *rsdec Reference Page*. URL `http://www.mathworks.com/help/comm/ref/rsdec.html`.

[41] V. Guruswami and M. Sudan. Improved decoding of Reed-Solomon and algebraic-geometric codes. In *Foundations of Computer Science, 1998. Proceedings. 39th Annual Symposium on*, pages 28–37, Nov 1998. doi: 10.1109/SFCS.1998.743426.

[42] R. Koetter and A. Vardy. Algebraic soft-decision decoding of Reed-Solomon codes. *Information Theory, IEEE Transactions on*, 49(11):2809–2825, Nov 2003. ISSN 0018-9448. doi: 10.1109/TIT.2003.819332.

[43] E.R. Berlekamp. *Algebraic Coding Theory*. McGraw-Hill series in systems science. Aegean Park Press, 1984. ISBN 9780894120633.

[44] Robert J McEliece. The Guruswami-Sudan Decoding Algorithm for Reed-Solomon Codes. *IPN progress report*, pages 42–153, 2003.

[45] Helmut Hasse. Theorie der höheren Differentiale in einem algebraischen Funktionenkörper mit vollkommenem Konstantenkörper bei beliebiger Charakteristik. *J. Reine Angew. Math.*, 175:50–54, 1936.

[46] Gui-Liang Feng and K.K. Tzeng. A generalization of the Berlekamp-Massey algorithm for multisequence shift-register synthesis with applications to decoding cyclic codes. *Information Theory, IEEE Transactions on*, 37(5):1274–1287, Sep 1991. ISSN 0018-9448. doi: 10.1109/18.133246.

[47] T. Bayes. An essay towards solving a problem in the doctrine of chances. *Phil. Trans. of the Royal Soc. of London*, 53:370–418, 1763.

[48] J. Justesen. Upper Bounds on the Number of Errors Corrected by the Koetter-Vardy Algorithm. *Information Theory, IEEE Transactions on*, 53(8):2881–2885, Aug 2007. ISSN 0018-9448. doi: 10.1109/TIT.2007.901169.